의학박사 학위논문

Novel molecular determinants contributing to the voltage dependent gating of CLC-1 channel

CLC-1 이온통로의 막전압 의존성 개폐의 조절기전

2017 년 02 월

서울대학교 대학원

의과학과 의과학 전공

하 꽃 다 지

A thesis of the Degree of Doctor of Philosophy

CLC-1 이온통로의 막전압 의존성 개폐의 조절기전

Novel molecular determinants contributing to the voltage dependent gating of CLC-1 channel

February 2017

The Department of Biomedical Sciences,
Seoul National University
College of Medicine
Kotdaji Ha

Novel molecular determinants contributing to the voltage dependent gating of CLC-1 channel

By Kotdaji Ha

A thesis submitted to the Department of Biomedical Science in partial fulfillment of the requirements for the Degree of Doctor of Philosophy in Biomedical Science at Seoul National University College of Medicine

February 2017

Approved by Thesis Committee:

Professor _____Chairman
Professor _____Vice chairman
Professor _____
Professor _____
Professor _____

ABSTRACT

The CLC family of proteins consists of channels and transporters that share similarities in architecture and play essential roles in physiological functions. Among the CLC family, CLC-1 channels have the representative homodimeric double-barreled structure carrying two gating processes. One is protopore gating that acts on each pore independently by glutamate residue (E_{ext}). The other is common gating that closes both pores simultaneously in association with large conformational changes across each subunit. In skeletal muscle, CLC-1 is associated with maintaining normal sarcolemmal excitability, and a number of myotonic mutants were reported to modify the channel gating of CLC-1. In this study, we characterized highly conserved helix O as a key determinant of structural stability in CLC-1. Supporting this hypothesis, myotonic mutant (G523D) at N-terminal of Helix O showed the activation at hyperpolarizing membrane potentials with a reversed voltage dependency. However, introducing glutamate at serine residue (S537) at the C-terminal of the helix O on G523D restored WT like voltage dependency of the common gate and showed proton insensitive voltage dependency. To further validate this significant site, site-specific mutagenesis experiments was performed on V292 that is highly conserved as glutamate in antiporter and closely located to S537 and

showed this area is essential for channel function. Taken together, the results of study suggest the importance of helix O as the main contributor for stable structure of evolutionary conserved CLC proteins and its key role in voltage dependency of the CLC-1. Furthermore, the C-terminal of the helix O can offer a clue for possible proton involvement in CLC- 1 channel.

This work was published in *Pflugers Arch. Feb;469(2):183-193*

Keywords: ClC-1, Helix O, voltage gated chloride channel, proton, channel gating, myotonia congenita

Student number: 2014-30672

CONTENTS

LIST OF TABLES AND FIGURES

LIST OF ABBREVIATION

CLC-1: Chloride Channel-1

KO: Kock out

CBS: Cystathionine beta synthase

TAL: Thick Ascending limb

CamKⅡ: Ca2+/calmodulin-dependent protein kinase Ⅱ

NCL: Neuronal ceroid lipofuscinosis

stCLC: Salmonella thyphimurium CLC

CLC-ec1: CLC-Escherichida coli

cmCLC: Cyanidioschyzon merolae CLC

Introduction

Chloride channels are reported to play important roles in various cellular functions (Jentsch *et al*., 1990), such as regulation of cell volume (Worrell *et al*., 1989), transepithelial transport (Gogelein *et al*., 1988) and stabilization of membrane potential in muscle (Bretag., 1987). Among chloride channels, the first CLC was isolated from the electric ray *Torpedo marmorata* in 1990 (Jentsch *et al*., 1990). Since firstly purified, it became to consist a chloride channel (CLC) family which includes both passive Cl^- channel and secondary active H^+ couped Cl^- antiporters (Han *et al*., 2013). To date, CLC-1, CLC-2, CLC-Ka and CLC-Kb were reported to function as channel whereas CLC-3 through CLC-7 function as exchangers (Stolting *et al*., 2014). These CLC proteins are ubiquitously expressed in most tissues, serving pivotal roles in a wide range of physiological tasks (Hille, 1992; Imbrici *et al*., 2015; Steinmeyer *et al*., 1991; Jentsch, 2008; Stolting *et al*., 2014).

Although divided into two groups operating with different thermodynamic principles, the CLC family shares a similar architecture in common. Crystallographic structure of CLC antiporter from *Salmonella typhimurium* (StCLC) and *Escherichia coli* (CLC-ec1) revealed the double-barreled architecture of CLC proteins originally suggested by electrophysiological studied (Ludewig *et al*., 1996; Middleton *et al*., 1996; Dutzler *et al*., 2002) (**Fig. 1a,b**). The homodimers consist of a subunit with 18 alpha helix domains named A (the first domain located in the cytosol) to R (the last domain located in the cytosol) (**Fig. 1c**). CLC channels and CmCLC have a cyotosolic cystathionine-β-synkthase (CBS)

domains, which is a common characteristic in eukaryotic CLC proteins whereas CLC-ec1 misses most of cytosolic part (Park *et al*., 2016).

Studies on CLC-ec1 showed that the side chain of a conserved glutamate residue (E_{ext}) at helix F competes with the Cl^- ions to occupy External anion binding site (S_{ext}), working as an external gate for anion (Accardi., 2015; Dutzler *et al*., 2003; Dutzler *et al*., 2002), while conserved tyrosine residue (Y_{cen}) at helix R plays a role as an inner gate (Bennetts *et al*., 2013). At the inner site, a Cl^- ion is specifically coordinated by four regions (**Fig. 1d**). The most conserved amino acids, GSGIP (106-110), G(K/R)EGP (146-150), GXFXP (355-359), Y (445) form a selectivity filter to diffuse anion down to the intracellular side (Dutzler *et al*., 2002).

a

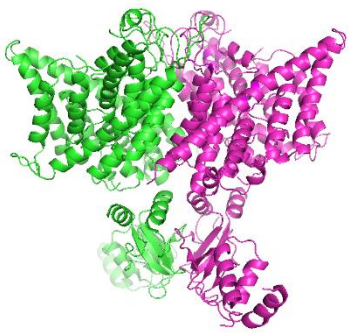

b

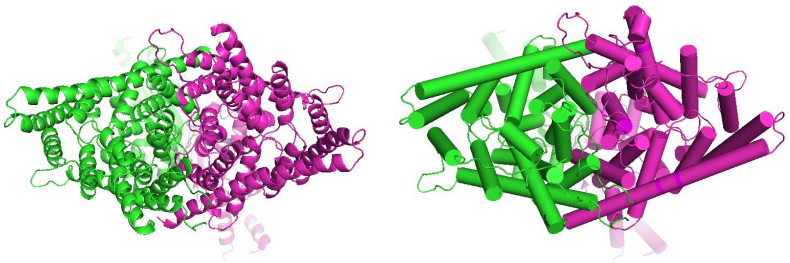

c

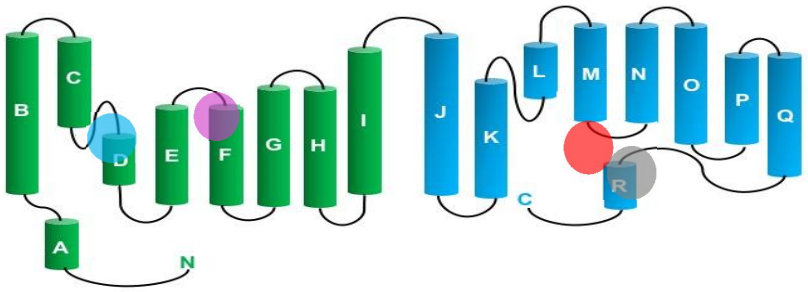
A
B
C
D
E
F
G
H
I
J
K
L
M
N
O
P
Q
R
N
C

d

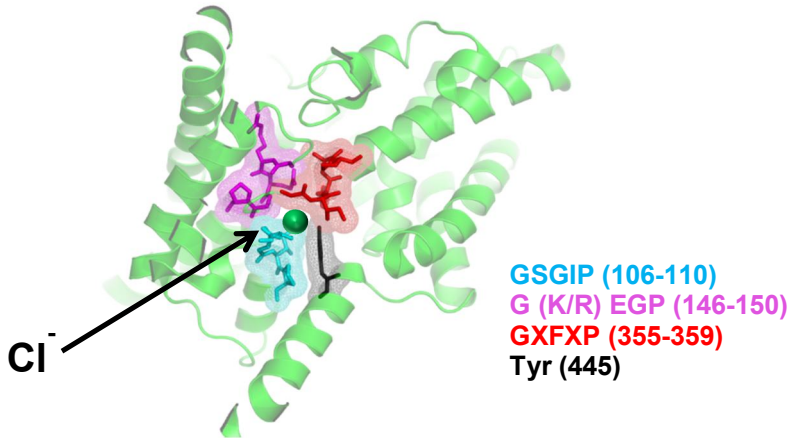
Cl-
GSGIP (106-110)
G (K/R) EGP (146-150)
GXFXP (355-359)
Tyr (445)

Figure 1. Homology modeling of CLC proteins based on the crystal structure of CLC-ec1 and cmCLC. Homology modeling describes the homodimeric architecture of CLC proteins. Each monomer was colored in green and magenta. Side view (**a**) and top view (**b**) were shown in ribbon (left) and cylinder (right) representation. (**c**) Topology drawing of CLC proteins. The □-helices (A domain to R domain) are described in cylinders and the regions of the conserved amino acids that consist of anion selectivity filter are indicated in cyan (GSGIP), magenta (G(K/R)EGP), red (GXFXP), and black (Y). (**d**) Cartoon of anion selectivity filter. The anion selectivity is formed by the conserved amino acids. The green sphere indicates a Cl^- ion.

Recent work on the eukaryotic CLC antiporter, cmCLC, suggested that the side chain of E_{ext} locates at a unique position, occupying central Cl^- binding site and forming a hydrogen bond with the central tyrosine (Y_{cen}) (Feng *et al*., 2010). In proton-transport of CLC antiporter, both internal glutamate residue (E_{int}) and E_{ext} are engaged in the exchange of 2 Cl^- for 1 H^+ (Lim *et al*., 2009; Feng *et al*., 2010; Feng *et al*., 2012). These stoichiometrical exchange Cl^- for H^+ occurs through a cycle of conformational modifications, but the essential part of this system still remains unveiled (Miller., 2006).

1. CLC-1

CLC-1 is a voltage dependent chloride channel which consists of 988 (human) and 994 (mouse) amino acids in length and exclusively expressed in skeletal muscle (Steinmeyer *et al*., 1991). In skeletal muscle, high Cl^- conductance (Gcl) accounts for ~85% of all membrane conductance, contributing stabilization of the membrane potential and repolarization of action potential (Bretag., 1987). The specific localization of ClC-1 in skeletal muscle cell still needs to be investigated to find whether ClC-1 presents in the sarcolemma or in the t-tubules (Aromataris *et al.*, 2006). However, some reports detected its expression in the sarcolemmal membrane (Gurnett *et al*., 1995; Papponen *et al*., 2005).

Since ClC-1 serves a pivotal role in the regulation of action potential in the skeletal muscle, its mutation can lead to the pathological condition called myotonia congenita. Myotonia congenita is an inherited genetic disease caused by the mutations in the gene (CLCN1) encoding CLC-1 (Pusch., 2002). Myotonia congenita can be characterized as autosomal dominant type (Thomsen's disease) and autosomal recessive type (Becker's disease) (Koch *et al*., 1992; George *et al*., 1993). Their common clinical symptoms can be described as a hyperexcitability of the skeletal muscle caused my repetitive firing of action potentials, which is called myotonic run (Jentch, 2001; Pusch., 2002). The patients who suffer from this medical condition display prolonged muscle contraction or muscle stiffness (Bretag., 1983; Pusch., 2002). To date, more than 100 different mutations in the CLCN1

gene have been reported to be responsible for myotonic condition (Lee *et al*., 2013), altering the channel function.

The structure of CLC-1 still remains uncovered. However, its electrophysiological characteristic has been identified and the structure of a CLC-K channel revealed by cryo-electron microscopy supports the notion that CLC-1 also consists of homodimers with each subunit conducting a separate Cl^-transport pathway (Park *et al*., 2016).

The function of CLC-1 channel is well described by two distinct gating processes; “fast gating (protopore gating)” and “slow gating (common gating)”(Steinmeyer *et al*., 1994). The separation of two gating mechanisms was conducted using a highly depolarizing potential in CLC-0 (Accardi and Pusch., 2000). A protopore gate regulates each pore independently, while a common gate simultaneously opens or closes both protopores (Accardi and Pusch., 2000). The fast gating works on the milli second timescale, and regulates the pore within each subunit of the CLC-0 dimer independently (Lisal and Maduke., 2008). On the other hand, slow gating regulates both pores at the same time on a time scale of seconds (Lisal and Maduke., 2008). It was previously reported that the side chain of E_{ext} is responsible for the protopore gate of CLC-1 at S_{ext} (Miller., 2006). However, mechanism of the common gating process is currently not well understood at the molecular level (Feng *et al*., 2010; Feng *et al*., 2012). Recently, it was suggested that the CBS (cystathionine-β-synthase) domain and Y_{cen} on helix R were engaged in common gating process (Bennetts *et al*., 2013).

2. CLC proteins

The various CLC proteins display a wide variety of gating and anion permeation characteristics. As aforementioned, CLC proteins can be grouped into channel and antiporter. CLC-1, CLC-2, CLC-Ka and CLC-Kb are grouped into channel type, and CLC-3 through CLC-7 are considered as antiporter.

CLC-2 is a broadly expressed in many epithelia, neurons, glia, and heart, and has a characteristic of inwardly rectifying plasma membrane Cl- channel (Thiemann *et al*., 1992). Loss of CLC-2 results in retinal and testicular degeneration (Bosl *et al*., 2001, Nehrke *et al*., 2002). In addition, a widespread vacuolation of the white matter in the brain and spinal cord was observed in CLC-2 KO mice (Blanz *et al*., 2007).

CLC-K channels and subunit β barttin are majorly involved in salt transport across the plasm membrane (Uchida *et al*., 1995; Vandewalle *et al*., 1997; Simon *et al*., 1997; Matsumura *et al*., 1999). Subunit β barttin is suggested to have two transmembrane domains with longer carboxy terminus and required to activate CLC-K channels (Waldegger and Jentsch, 2000). Barttin activates CLC-K channels by increasing the surface expression of CLC-K proteins that majorly distributed in the endoplasmic reticulum (Estevez *et al*., 2001; waldegger *et al*., 2002; Hayama *et al*., 2003; Scholl *et al*., 2006; Jentsch, 2008). CLC-K channels are mostly localized in the kidney (Uchida *et al*., 1995; Vandewalle *et al*., 1997; Estevez *et al*., 2001; Kobayshi *et al*., 2001) and the inner ear (Estevez *et al*., 2001).

Specifically, CLC-Ka and -Kb are expressed in the basolateral and apical membrane of the thin limb of Henle's loop and only basolateral membranes of the thick ascending limb of Henle's loop (TAL), the distal convoluted tubule, and collecting duck, respectively. They are also detected in the basolateral membranes of marginal cells of the stria vascularis. Clinical symptoms of mutations in CLC-K channels display human Bartter syndrome type, Ⅲ,Ⅳ, and deafness.

On the other hand, CLC exchangers are majorly placed in the intracellular organelles such as endosomes and lysosomes to facilitate luminal acidification or regulate luminal chloride concentration (Jentsch, 2016). CLC-3 is localized in the membrane of endocystc system (Miller *et al*., 2007) as well as in synaptic vesicles (Salazar *et al*., 2004). CLC-3 is suggested to produce swelling-activated chloride current (Duan *et al*.,1997) and modulate excitatory synaptic transmission in the hippocampus as a Ca^{2+}-dependent, CamKⅡ-activated Cl- channel (Wang *et al*., 2006). CLC-3 KO mice display a postnatal degeneration of the hippocampus and retina (Stobrawa *et al*., 2001).

CLC-4 is ubiquitously expressed in a number of tissues (Jentsch *et al*., 1995). CLC-4 was thought to have characteristics of channel, but it is now considered as voltage- dependent electrogenic Cl-/H+ exchanger (Picollo and Pusch, 2005). The clinical symptom or pathological aspects of CLC-4 still remains unclear and it needs to be further investigated.

CLC-5 is also a Cl-/H+ exchanger responsible for renal

endocytosis and prominently localized in the epithelia of kidney and intestine (Steinmeyer *et al*., 1995, Vandewalle *et al*., 2001). Clinically, mutations in CLC-5 result in Dent's disease of which symptom display recurrent kidney stones and nephrocalcinosis (Wrong *et al*., 1994). It is suggested that CLC-5 protein plays a key role in the proximal tubular endocytosis and acidification of renal endosomes (Piwon *et al*., 2000).

CLC-6 is a late endosomal neuronal chloride transporter that plays a pivotal role in lysosomal function. It still remains controversial weather CLC-6 is a channel or exchanger, but there is a possibility that CLC-6 is considered as an exchanger due to existence of "proton glutamate" that only present in CLC Cl^-/H^+ exchangers (Accardi *et al*., 2005). CLC-6 is mainly expressed in dorsal root ganglia and CLC-6 KO mice revealed a lysosomal storage disease and mild form of human neuronal ceroid lipofuscinosis (NCL) (Jentsch, 2016). It was previously reported that the patients who suffer from late onset NCL were screened to have mutations in CLCN6 (Poet *et al*., 2006).

CLC-7 is a lysosomal Cl^-transporter serving crucial tasks in lysosomes and osteoclasts. The physiological roles of CLC-7 were revealed via generation of KO mice that showed the symptom of severe osteopetrosis, calcification of bone marrow cavities, and degeneration of the retina (Kornak *et al*., 2001). So far, more than 30 mutations of CLCN7 encoding CLC-7 were reported to cause human osteopetrosis (Frattini *et al*., 2003; Waguespack *et al*., 2003; Waguespack *et al*., 2007).

3. The aim of this study

Development of myotonia congenita is associated with the malfunction of the CLC-1 protein. In particular, many pathogenic mutants display abnormal voltage dependency in the common gating function (Pusch., 2002). Known myotonic mutants, G523D and G499R, each located on helix O and helix N of human CLC-1, respectively, were previously reported to exhibit increased activation at hyperpolarized membrane potentials, where wild type hCLC-1 is rapidly deactivated (Zhang *et al*., 2000; Ha *et a*l., 2014). Intriguingly, reversed voltage-dependency of the common gating of G523D mutant is similar to the changed voltage-dependency of wild type CLC-1 at a low extracellular pH (Zhang *et al*., 2000; Ha *et al*., 2014), which may indicate the involvement of protons in the voltage-dependency of the common gate.

Movement of helix O was reported to be important in the inner gate (Y_{cen}) movement via a direct interaction of its C-terminal end (I402) and Y_{cen} in CLC-ec1 (Basilio et al., 2014). Unlike CLC-ec1, serine (S537) places at the corresponding position of I402 in hCLC-1. S537 and its surrounding cavity were identified as an inhibitor binding site by previous studies (Bennetts and Parker, 2013; Estevez *et al*., 2003).

In this study, I hypothesized that S537 residue on helix O in hCLC-1 plays a crucial role in the voltage-dependency of the channel gate by sensing extracellular pH. Mutations at S537 at the C-terminal of helix O restored WT-like channel behavior in the mutants that exhibited reversed voltage dependency, thereby contributing to the conformational stability. Furthermore, the effect of E_{int}-restoring mutant, V292E on S537 was also investigated to observe structural conservation with respect to key gating residues, Y578 (Y_{cen}) and E232 (E_{ext}) in CLC-1 by structural modelling. Collectively, the data suggest that helix O participates in the conformational stability of CLC-1 channel, modulating the voltage dependency and proton involvement can be linked to this phenomenon. The data also support that partial role swapping between S537 and V292 is a key step in the evolution of CLC channels.

Study Strategy Scheme

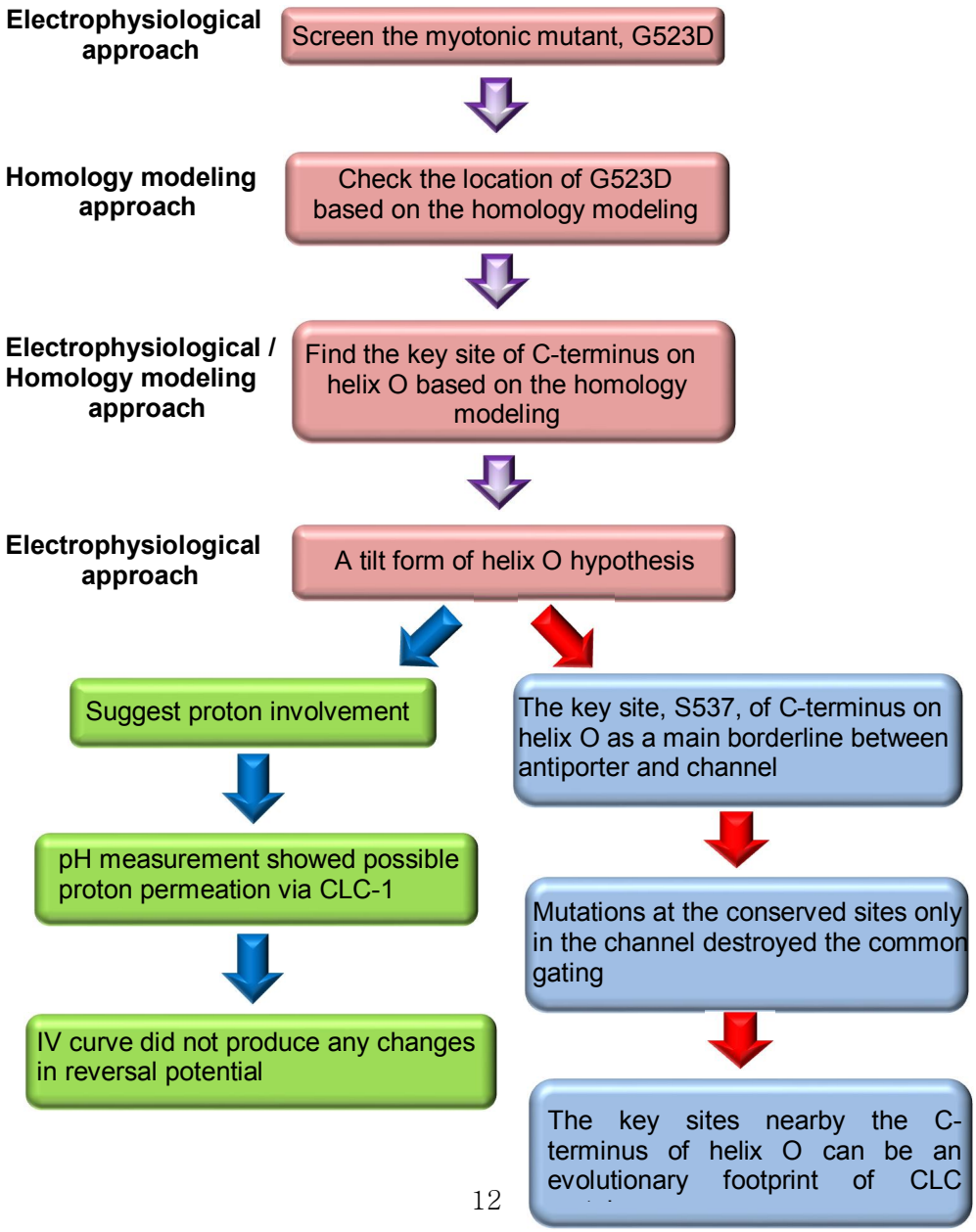

Salt bridge between helix B and F

Figure 2. Study strategy scheme.

Materials and Methods

1. Construct.

Human CLCN1 DNA in the pRc/CMV vector was subcloned into the pEGFP-N1 vector (Clontech) using the enzyme site Xho1 and EcoR1. The mutants were created by employing the QuickChange site-directed mutagenesis kit (Stratagene), followed by DNA sequence verification. hCLCN1 gene was provided in kind by Dr. Alfred. L. George of Vanderbilt University, Nashville, TN. U.S.A.

2. Cell Culture and DNA Transfection.

HEK293 cells were grown in Dulbecco's modified Eagle's medium (DMEM) supplemented with 10% fetal bovine serum (Hyclone) and 1% penicillin and incubated at 37°C in a humidified incubator with 95% air and 5% CO_2. Transient transfection was conducted by using Fugene 6 (Promega).

3. Homology modelling.

Homology model of hCLC-1 was rendered using proved crystal structure of cmCLC (PDB id: 3ORG) which has 97% of query cover and 31% identical residues and stCLC (PDB id: 1KPL) with 87% of query cover and 25% identical residues when compared to the

transmembrane domain of the hCLC-1. Crystal structure of the C-terminal domain of CLC-0 (PDB: 2D4Z) was also used, which shares 40% identical residues and 70% query cover when compared to the C-terminal domain of hCLC-1. MODELLER was used to construct the CLC-1 model and all the figures were prepared using Pymol 1.8.0.5[12]. N-terminal domain of the model was omitted due to lack of similar crystal structure in the N terminus.

4. Electrophysiology & Data analysis.

Human CLC-1 gene (CLCN1) was carried in vector pEGFP-N1 and was overexpressed in HEK293 cells using fugene6 transfection reagent. Patch clamp experiments in the whole cell configuration were performed in the room temperature. Axopatch 200B amplifier and Digidata1440 with software Clampex were used for current recording. Cells were bathed in solution containing in mM: 140 NaCl, 4 KCl, 2 $CaCl_2$, 1 $MgCl_2$, 5 HEPES, adjusted with NaOH to pH 7.4. For low pH bath solution, MES was used as a substitute for HEPES, and the pH was adjusted with NaOH. Intracellular solution were composed of : 130 NaCl, 2 $MgCl_2$, 5 EGTA, 10 HEPES, adjusted to pH 7.4 with NaOH. Open probabilities were fitted with a *Boltzmann* distribution with some modifications.

$$P_o(V)=P_{-165}+(P_{+75}-P_{-165})/(1+\exp[(V_{1/2}-V)/\kappa]) \qquad (1)$$

where P_{-165} and P_{+75} are the open probabilities of the channel at most negative potential (-165mV) and most positive potential (+75mV) each, V is the membrane potential, $V_{1/2}$ is the half-maximal activation potential, and κ is the slope factor. Time constants of steady-state activation of G523D hCLC-1 were determined by fitting bi-exponential functions to the time dependence of current amplitudes.

To separate fast and slow gating process open probability, the following

equation (2) was introduced.

$I(V_p) = Ni_{-125}P^s_o(V_p)P^f_o(V_p)$ (2)

Where $P_o^s(V_p)$ and $P_o^f(V_p)$ are the open probabilities of the common (slow) and protopore (fast) gating process, respectively. *N* and i_{-125} indicate the number of channels expressed on the cell and the single channel amplitude obtained at -125 mV, respectively. After applying voltage step protocol from -165 mV to 75 mV in 20 mV steps, a short 15 ms prepulse to +175 mV that maximally activates the protopore gate is applied. Thus, it is assumed that $P^f_o(max)$ ~1, and the following equation (3) can be deduced.

$I_{pp}(V_p) = Ni_{-125}\ P_o^s(V_p)$ (3)

where $I_{pp}(V_p)$ indicates the current obtained when prepulse was given and normalization of this current is equivalent to $P_o^s(V_p)$. Based on the equations above, the following equation is drawn.

$I(V_p)/\ I_{pp}(V_p) = P^f_o(V_p)$ (4)

To further test the separation of protopore and common gate, the currents of G523D mutant were analyzed using the protocol used for CLC-2 (de Santiago *et al.*, 2005). The voltage pulses were given from +75 mV to -165 mV in 20 mV increments and an interpulse, -200 mV was inserted for 15 ms. After the interpulse, the same test voltages were applied with +60 mV tail pulse followed. Since the steady-state of CLC-2 currents consists of protopore and common gating, the following equation is introduced.

$I_{Cl1} = 2NiP_sP_f$ (5)

where I_{Cl1} indicates the currents obtained at the end of the test voltage. We also hypothesized that 15 ms interpulse maximally activates the fast gating determining P_f as ~1. Assuming the interpulse to -200 mV does not affect the common gate, the initial currents obtained by the test voltage pulses can be considered as:

$I_{Cl2} = 2NiP_s$ (6)

Therefore, P_f can be deduced by I_{Cl1}/I_{Cl2} for CLC-2.

5. Fluorescence microscopy.

Cells were imaged on a Nikon Eclipse T*i* after transfection. During pH measurement experiment, cells were incubated with physiologic solution (mM): NaCl 140, KCl 4, $CaCl_2$ 2, $MgCl_2$ 1, HEPES 5 with pH 7.4, and subsequently perfused with 30 mM sodium acetate and 30 mM ammonium chloride added to the physiologic solution to induce intracellular pH modification. The imaging experiment was conducted for 3 mins and all the images were collected during excitation at 400 nm and emission at 500 nm, respectively. Data were analyzed using Metamorph software (Universal Imaging, Downingtown, PA). Background fluorescence was subtracted from cell fluorescence and relative fluorescence was obtained after normalization of cell fluorescence.

Results

1. Mutations on the N-terminus of helix O cause reversed voltage-dependency in the channel gate

Among previously reported myotonic mutants, some mutants show unique characteristics that shows channel activation upon hyperpolarizing pulses (Ha *et al*., 2014; Zhang *et al*., 2000). In the previous study, It was previously reported a novel myotonic mutant G523D, which activates upon membrane hyperpolarization (**Fig. 3a**) (Ha *et al*., 2014). G499R mutant was also reported to be activated by hyperpolarized membrane potential (Zhang *et al*., 2000). Although the mutants have the opposite charges they produced similar effects in channel gating. To study the effect of charged mutations, homology modeling was built (**Fig. 3b,c**), thereby suggesting that the aspartate side-chain of G523D is expected to interact with nearby loop between two helices N and O. G499 on helix N is closely located to the helix O and introduced arginine at this position possibly forms hydrogen bond with the carbonyl backbone of P521 on helix O **(Fig. 3b,c)**. Sequence alignments of these mutation sites in conjunction with molecular modelling of CLC-1 based on the structure of cmCLC revealed how much they are conserved and where they are located (**Fig. 4**). Thus,

structural modelling suggests that possible conformational change of helix O caused by charged mutations might cause the reversed voltage-dependency of the gating process.

For further validation of commonly mutated into charged amino acids, negatively charged mutations were introduced in G523. Interestingly, G523E induced reversed voltage-dependency in the channel gate compared with wild type CLC-1 (**Fig. 3a**). In contrast, G523R and G523Q mutants resulted in wild type-like voltage sensing which activates upon membrane depolarizing potential and open probabilities (**Fig. 5**). It is also noteworthy that WT CLC-1 shows reversed voltage-dependency at low extracellular pH condition as myotonic mutant G523D (**Fig. 3a**), suggesting that possible proton contribution in the activation of CLC-1 channel upon hyperpolarized potentials. G523D, G499R and WT CLC-1 at the low extracellular pH condition induced kinetically similar currents and gating process. As a consequence, it was suggested that they share the similar conformational arrangements of helix O in response to their gating function, and proton might be engaged in this structural stability.

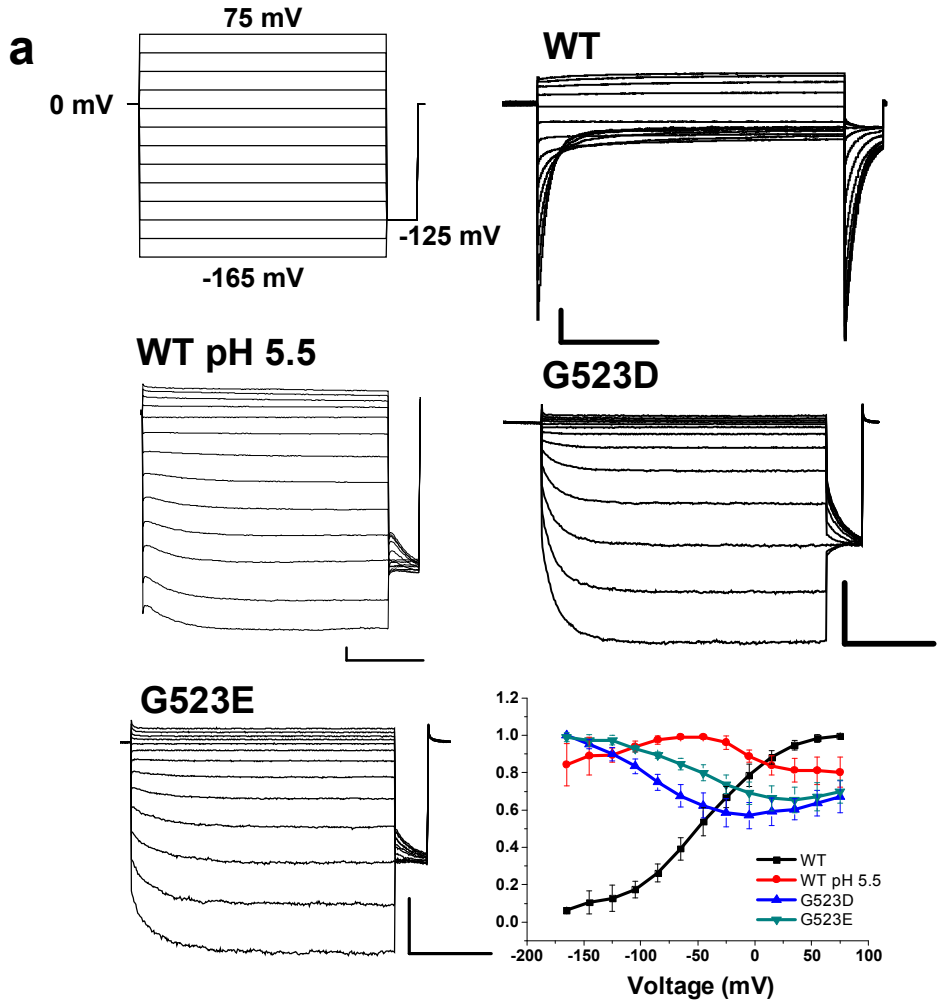
a
75 mV
0 mV
-125 mV
-165 mV
WT
WT pH 5.5
G523D
G523E
1.2
1.0
0.8
0.6
0.4
0.2
0.0
-200
-150
-100
-50
0
50
100
Voltage (mV)
WT
WT pH 5.5
G523D
G523E

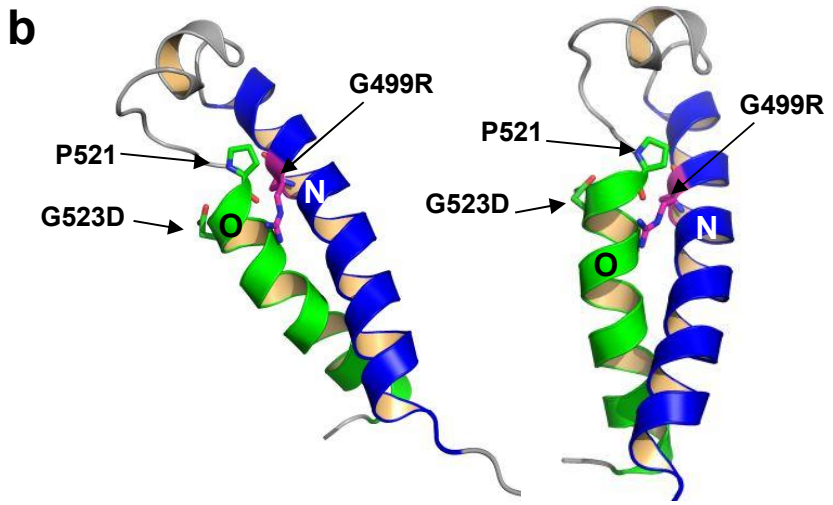

Figure 3. Mutations on the N-terminus voltage dependency

a.b. Molecular model showing location of G523D on helix O and G499R on helix N that cause activation at hyperpolarized membrane potentials. Homology models of CLC-1 are illustrated based on the structure of cmCLC (PDB id: 3ORG) and stCLC (PDB id: 1KPL). Helices O and N are colored in green and blue, respectively. The side chains of the mutated residues are shown as sticks colored in magenta. The molecular model suggests a new hydrogen bond interaction between G499R on helix N and P521 on helix O.

c. Step pulse protocol and representative whole cell current traces for wild type hCLC-1 under bath solutions of pH 7.4 or pH 5.5, G523D, and G523E, respectively. Dashed lines indicate zero-current level and scale bars indicate 0.5 nA (vertical) and 50 ms (horizontal). Open probabilities of apparent gating obtained from the tail current amplitude at -125 mV. Open probabilities of G523D (blue) and G523E (green) under extracellular pH 7.4 were compared with those of wild type

hCLC-1 under pH 7.4 (black) and pH 5.5 (red), respectively. Data are means ±s.e.m. n=4 (wild type hCLC-1), n=3 (wild type hCLC-1 under pH 5.5), n=6 (G523E), n=6 (G523D).

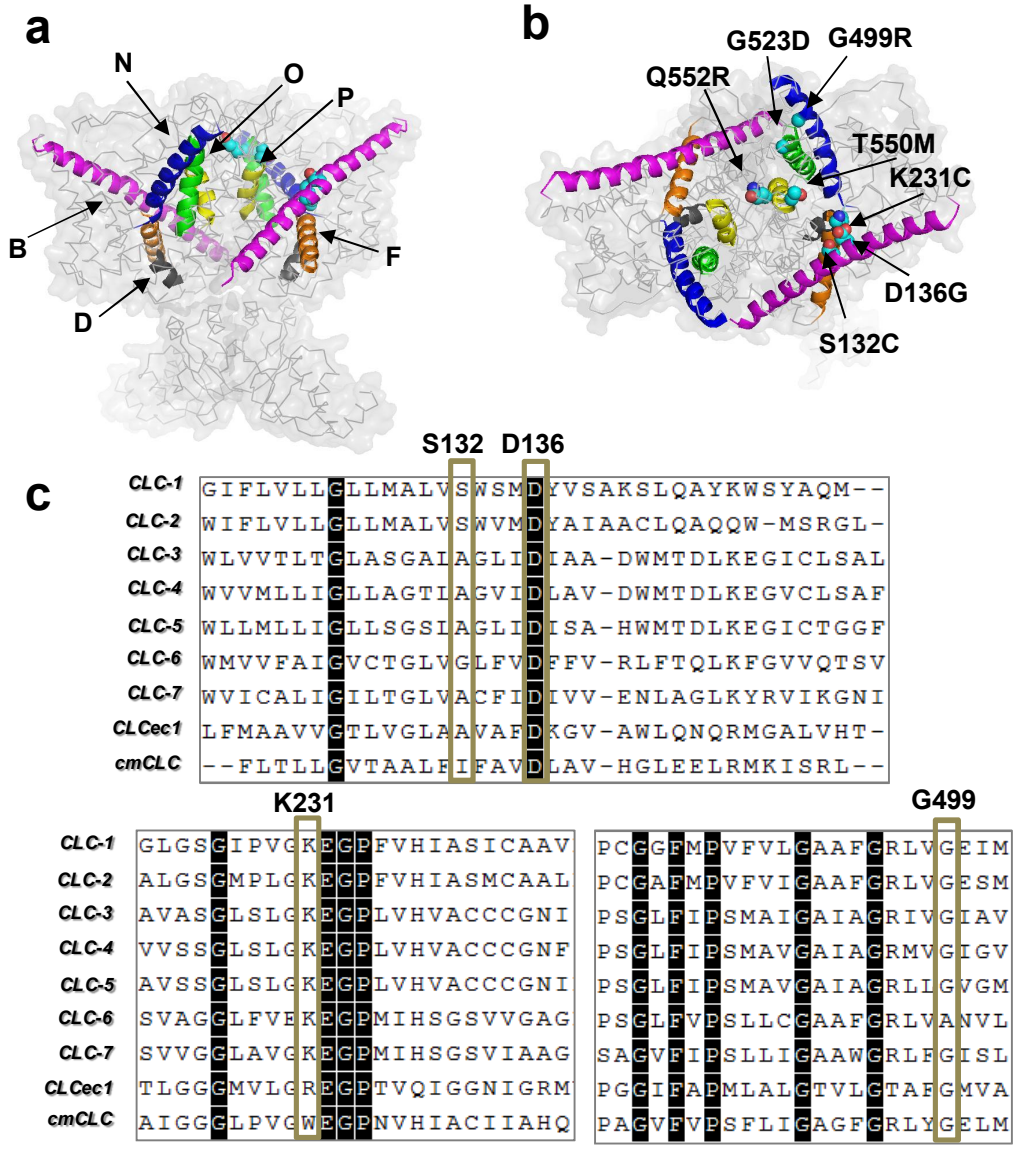

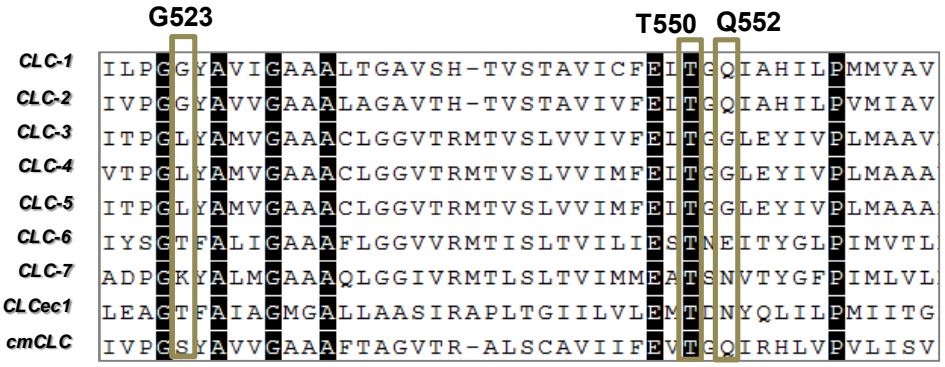

Figure 4. Molecular modelling of ClC-1 and sequence alignment of mutant sites.

a, **b.** Side (a) and top (b) views of the ClC-1 model that is built based on the structure of cmClC (PDB id: 3ORG) and stClC (PDB id: 1KPL). The helices related to the mutants activated at hyperpolarized potentials were highlighted in colors: helices B (pink), D (grey), F (orange), N (blue), O (green), and P (yellow). The positions of the residues on helices corresponding to mutations were depicted as space-filled model in cyan. **c.** Amino acid sequence alignments of the ClC family and the positions of the mutated residues. The sequence alignment was performed using MUSCLE (multiple sequence comparison by log-expectation) alignment implemented in MEGA 6.06 (Tamura, 2013). Conserved residues are highlighted with different colors based on their biochemical characteristics. The positions of the mutated residues were shown above the sequence alignments.

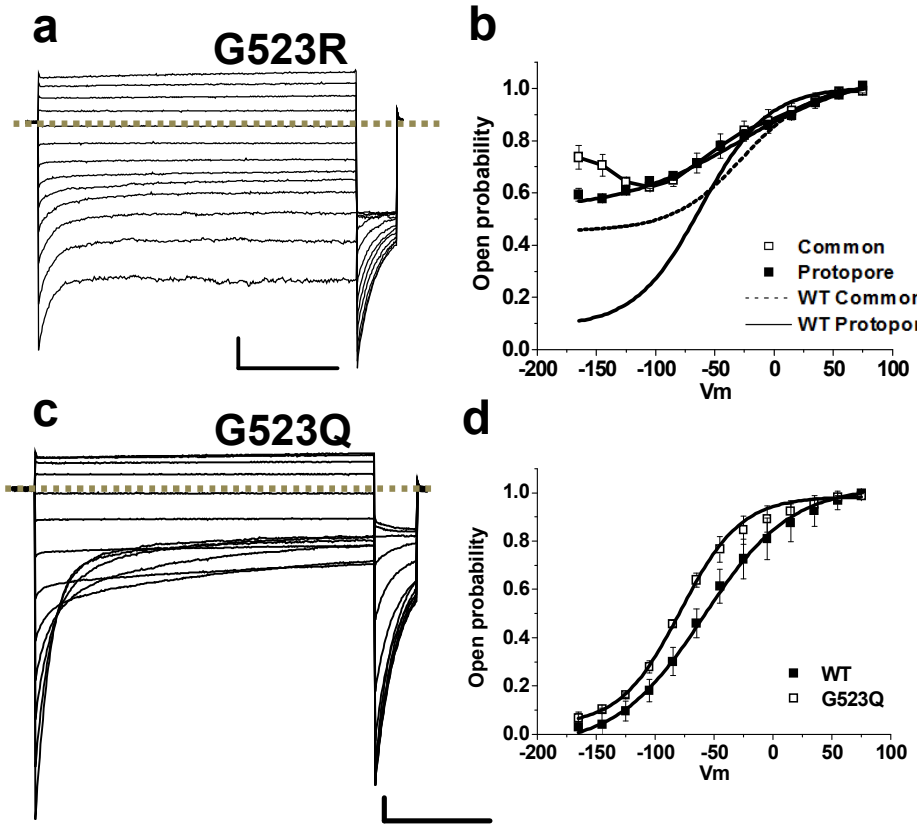

Figure 5. G523 mutants with normal voltage dependency.

a,c. Whole cell current traces for G523R and G523Q mutants. Dashed lines indicate the 0 current level with scale bar 50 ms (horizontal) and 0.5 nA (vertical). **b.** Open probabilities of the protopore and the common gate in G523R. Filled squares indicate the protopore gate open

probability, and blanked squares are for the open probability of the common gate which is not fitted to equation (1). Dashed and solid lines without data points indicate the open probability of the common gate and the protopore gate of the wild type ClC-1, respectively. **d.** Apparent open probabilities of the G523Q mutant and wild type ClC-1. Open probability was obtained from the tail current. All the data are expressed means ± s.e.m. n=2 (G523R and G523Q)

2. Gating Separation of myotonic mutant G523D

To evaluate the mechanism of this unique trait, the properties of a series of G523 mutants were examined by applying a voltage pulse protocol developed by *Accardi* and *Pusch,* 2000 and Stolting *et al*, 2014*b* that make it possible to separate common gate and protopore gate from macroscopic current recordings. To evaluate two kinetically distinct gating processes, the protocols used for CLC-2 and CLC-1 and CLC-2 hetero-dimeric channels were applied due to the similarity of electrophysiological traits of G523D and CLC-2 (de Santiago *et al*., 2005).

Although CLC-1 and CLC-2 have distinct electrophysiological characteristics from each other, G523D was activated upon hyperpolarized potentials with slow time constant similar to WT CLC-2. This phenomenon suggests that G523D shows similar channel kinetics to WT CLC-2, rather than WT CLC-1. To cement the analysis for the channel kinetics, the voltage pulse protocols for CLC-2 were applied to validate G523D CLC-1. To solve the technical concerns, two different voltage protocols for CLC-1 and CLC-2 with the prepulse at +170 mV or -200 mV were utilized to assess G523D. Based on the designed voltage protocols, the time constant was obtained to evaluate if two distinct gating process can be separated and it was revealed that two

distinct gating processes exists with different time constants **(Fig. 6a)**.

The currents of G523D obtained from -85 mV to -165 mV were fitted to biexponential equation **(Fig. 6b)** Based on the time constants obtained by fitting the currents at hyperpolarized potentials to biexponential equation, the time constant for the fast gate was determined to be 10 ms faster than the slow gate **(Fig.6a).** To characterize the relative open probability of the slow gate, the duration of a short hyperpolarizing pulse for 10 ms was given to fully activate fast gate **(Fig. 6c top).**

To cement this analysis, a short depolarization pulse to +175 mV for 15 ms was also inserted **(Fig. 6c. bottom)**. Two distinct voltage pulses applied to assess G523D mutant resulted in the similar voltage dependencies in the protopore and common gating. Collectively, these evaluations demonstrate that two kinetically different slow and fast gate can be separated, and G523D resulted in the reversed voltage dependency in both gates, which led us to corroborate that G523D on helix O plays a key role in conformational rearrangement and channel gating.

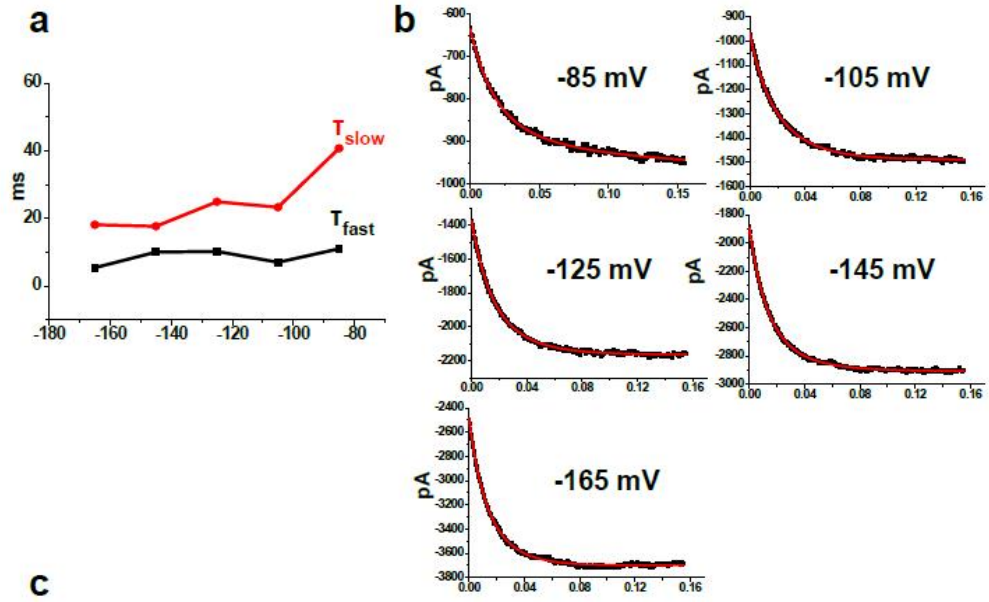
a
b
c
ms
60
40
20
0
-180
-160
-140
-120
-100
-80
T slow
T fast
pA
-85 mV
-105 mV
-125 mV
-145 mV
-165 mV
0.00
0.05
0.10
0.15
0.04
0.08
0.12
0.16

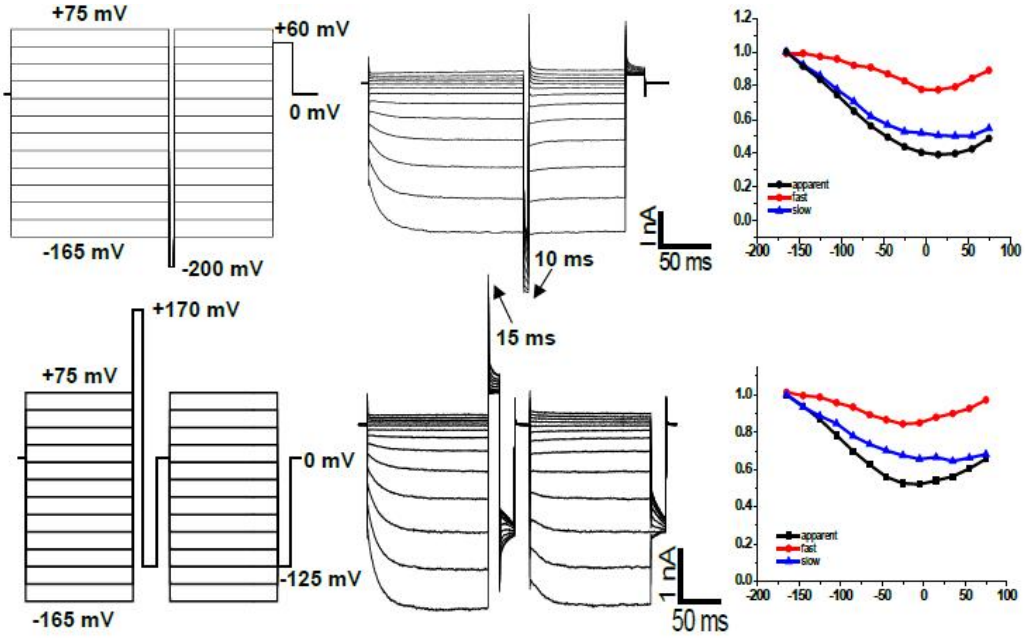

Figure 5. Gating separation test of G523D mutant

a. Time constants of the activation kinetics of G523D currents obtained by bi-exponential fits. **b.** Bi-exponential fitted currents from negative voltage pulses. Red line indicates bi-exponential fits. **c.** Voltage protocols utilized for common and protopore gating separation. The step pulses were given from -165 mV to +75 mV in 20 mV increments for 160 ms and a short hyperpolarization pulse to -200 mV for 10 ms was inserted. Holding potential was given at 0 mV (**top**). The step pulses were given from -165 mV to +75 mV in 20 mv increments for 160 ms and a short depolarization pulse to +175 mV for 15 ms was inserted (**bottom**). **d.** Representative whole cell currents obtained by each voltage protocol. **e.** Voltage-dependencies of the separated fast, slow and apparent gatings of G523D obtained from each voltage protocol, respectively.

3. S537 mutants restore wild type-like voltage dependency of myotonic G523D mutant

In the model (Dutzler *et al*., 2003; Feng *et al*., 2012), S537 at the C terminus of the helix O is located in the vicinity of the central chloride binding site (**Fig. 7a**). S537 corresponds to I402 in CLC-ec1, which serves as an inner gate with interaction of Y_{cen} to occupy the central chloride pathway (Basilio *et al*., 2014). In CLC-ec1, E202 and E203 (E_{int}), corresponding to E291 and V292 of hCLC-1, respectively, are known to be the key residues in proton transport pathway across CLC-ec1 (Lim *et al*., 2012). Based on the homology modelling structure of hCLC-1 and experiments done in Fig.1, it was hypothesized that

mutations on the N-terminus of helix O could shift its C-terminus and induce conformational changes in the central chloride pathway.

Thus, the effect of S537 mutations on G523D mutant channel was tested to find whether the distinct channel kinetics caused by mutation at N-terminus of helix O can be restored by mutation at C-terminus of helix O, participating in the conformational stability. To be surprised, S537 mutants on G523D indeed recovered voltage-dependency of the common gate compared to G523D alone (**Fig. 7c**). In addition, The $V_{1/2}$ of WT P_o^{common} (-28.9±12.7 mV) and S537E G523D double mutant P_o^{common} (-29.9±5.6 mV) were approximately similar (**Table1**). A single point mutations, S537E or S537R produced WT-like voltage-dependence of common gate, and S537G or S537Q caused a shallow voltage-dependence. (**Fig.8**).

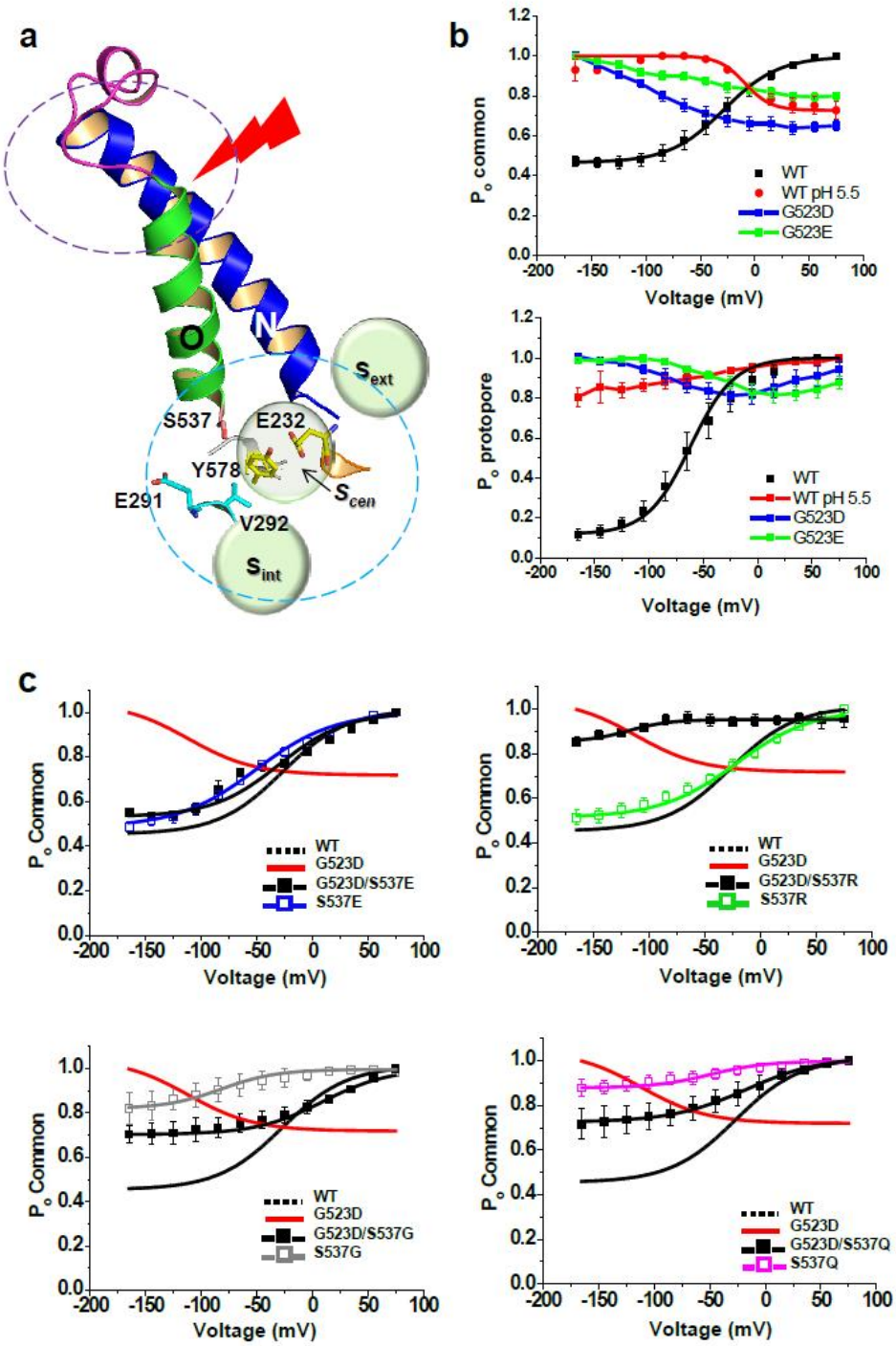

Figure 7. S537 mutants restore wild type-like voltage dependency

of G523D mutant.

a. Homology model illustrating helix O (green) and residues near S537. The S537 residue (pink) is located at the C-terminal end of helix O, and is adjacent to central anion binding site (S_{cen}) and Y578 (yellow) as well as E291 (cyan) and V292 (cyan). External (S_{ext}) and internal (S_{int}) anion binding sites are shown as spheres (orange) and the residues are displayed as sticks. **b**. Open probabilities of common and protopore gating. The gating separation was deduced using the method described by Accardi and Pusch, 2002 and Stolting et al, 2014b. Apparent open probability was obtained from the tail current amplitude at -125 mV. For the full activation of protopore gating, while marginally influencing common gating, a brief voltage pulse to +170 mV for 15 ms was inserted before the application of tail pulses. Open probabilities of G523D (blue) and G523E (green) under extracellular pH 7.4 were compared with those of wild type hClC-1 under pH 7.4 (black) and under pH 5.5 (red), respectively. Data are means ± s.e.m. n=4 (wild type ClC-1), n=3 (WT pH 5.5) n=6 (G523D), n=8 (G523E), n=10. **c**. Restoration of wild type-like voltage dependency by S537 mutations in G523D mutants. Black dashed line and red line represent the fit of the open probabilities of common gating of wild type ClC-1 and G523D, respectively. Closed black and open colored squares indicate means ± s.e.m. of the open probabilities of the double mutants and the single S537 mutants, respectively. n=7 (S537E, blue), n=4 (G523D/ S537E, S537R, green and S537G, grey) and n=3 (G523D/ S537R, G523D/ S537G, S537Q, magenta and G523D/ S537Q)

Table 1. Voltage dependent parameters of protopore and common

gates from WT and G523 and G523-S537 double mutants

	$V_{1/2}$	k	P_{min}
common gating			
WT CLC-1	-28.9±12.73	25.8±4.7	0.46±0.07
WT pH5.5	-5.9±1.7	10.9±2.5	0.73±0.03
G523D	-119.5±6.8	22.5±6.7	0.72±0.10
G523K	-102.5±21.6	40.6±10.3	0.58±0.02
G523E	-62.4±2.6	22.1±1.7	0.69±0.00
G523D S537E	-29.9±5.6	67.8±15.4	0.55±0.00
G523D S537R†	-	-	0.85±0.02
G523D S537G†	-	-	0.70±0.04
G523D S537Q†	-	-	0.72±0.07

	$V_{1/2}$	k	P_{min}
protopore gating			
WT CLC-1	-60.4±18.5	25.8±3.3	0.12±0.03
WT pH5.5	-60.3±37.6	60.0±17.6	0.80±0.05
G523D	-62.4±2.6	22.1±1.7	0.57±0.14
G523K	-9.9±28.7	26.3±11.1	0.81±0.05
G523E†	-	-	0.90±0.01
G523D S537E†	-	-	0.72±0.11
G523D S537R†	-	-	0.89±0.09
G523D S537G†	-	-	0.59±0.09
G523D S537Q†	-	-	0.65±0.02

Data show the parameters obtained by fitting a Boltzmann equation to Voltage dependent data from each gate. Data are means and s.e.m. † indicates the mutants that did not display voltage dependency.

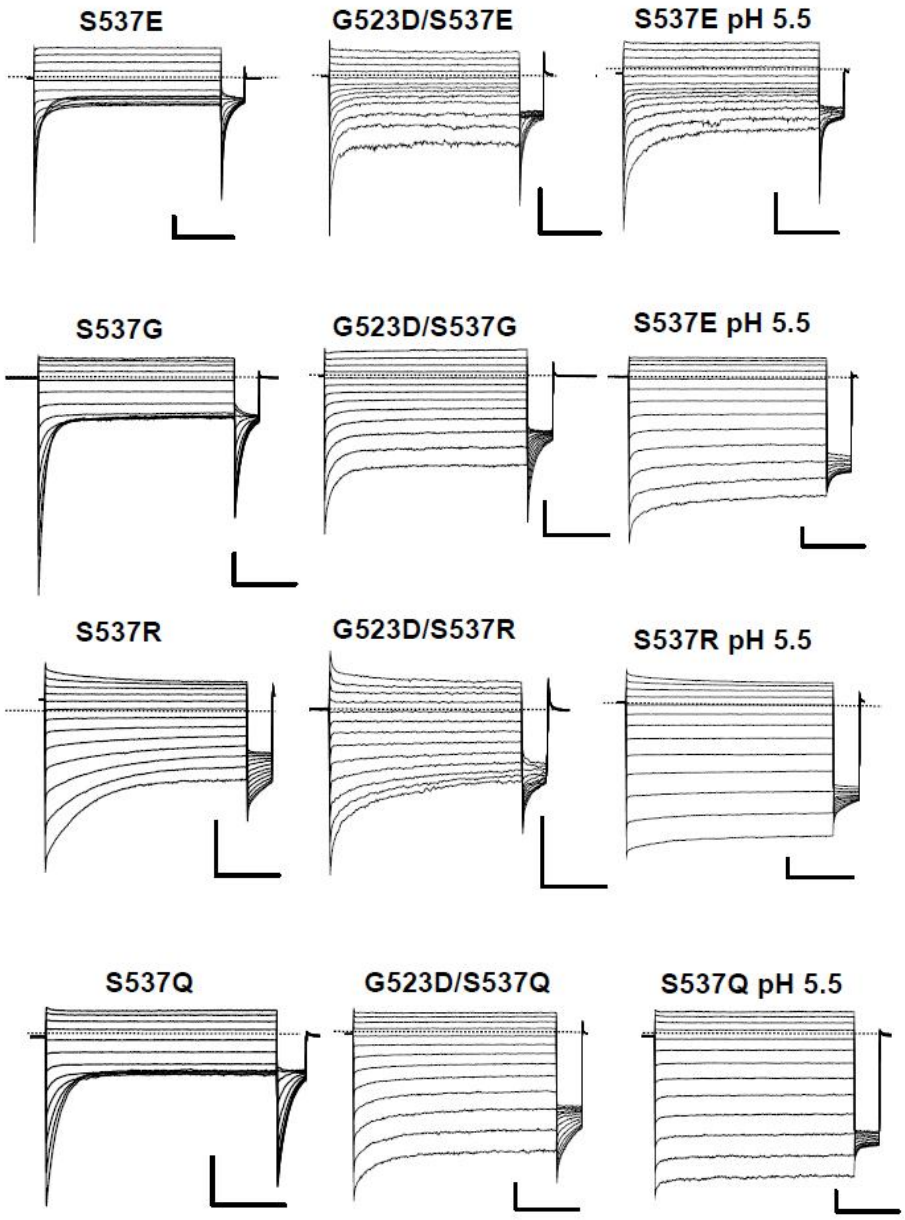

Figure 8. Whole cell current traces of the S537 mutants and the double mutants.

Whole cell current traces for S537/G523D double mutants and S537 single mutants under extracellular pH 7.4 or 5.5 conditions. Dashed lines indicate zero current level. Scale bars represent 0.5 nA in vertical and 50 ms in horizontal, respectively.

4. Titratable residue at S537 plays a significant role in channel gating under pH variation

S537X and G523D double mutant analysis suggested that the hyperpolarization-activated trait of G523D mutant was restored WT-like voltage dependency by S537 mutants, especially substituted with glutamate. As previously mentioned, WT CLC-1 under low extracellular pH condition might display a similar conformation to G523D mutant, and the electrophysiological characteristics of S537 mutants was compared under bath solutions of pH 7.4 with under pH 5.5 to reveal proton involvement at S537 site. Unlike wild type CLC-1, the common gate of the S537G and S537Q showed always active and S537R showed pH-dependent changes of voltage depolarization at extracellular pH 7.4 (**Fig. 9a**, **Fig. 5**).

To analyze the change occurring in the voltage-dependent common gating process in response to external pH changes (**Table2**), the open probabilities of the common gate was double substracted. ΔP was calculated from open probability (P_o) at membrane potential of 75mV subtracted with Po at -165mV (**Fig. 9b**). Then, ΔΔP was obtained by subtracting the ΔP under extracellular pH 5.5 from ΔP under extracellular pH 7.4 (**Fig. 9c**). Subtraction analysis clearly showed that the common gating of S537 mutants is significantly less affected by extracellular pH modification compared to wild type CLC-1 (**Fig. 9c**). In addition, the common gating of S537Q and S537G is almost voltage-independent under pH 7.4 as well as pH 5.5 with no significant difference regarding extracellular pH (**Fig 9a**). Collectively, S537 mutants did not sense extracellular pH change, thereby displaying unchanged voltage dependency unlike WT CLC-1 under pH 5.5 that shows reversed voltage dependency.

Thus, it was hypothesized that S537 is the key residue to sense

pH changes and the regulation of voltage dependency in common gate. Furthermore, the constitutively active common gate of mutant V292E closely located to S537 is also marginally affected by the extracellular proton concentration (**Fig. 10**). Therefore, S537 plays a key role in the normal function of the common gate by proton involvement.

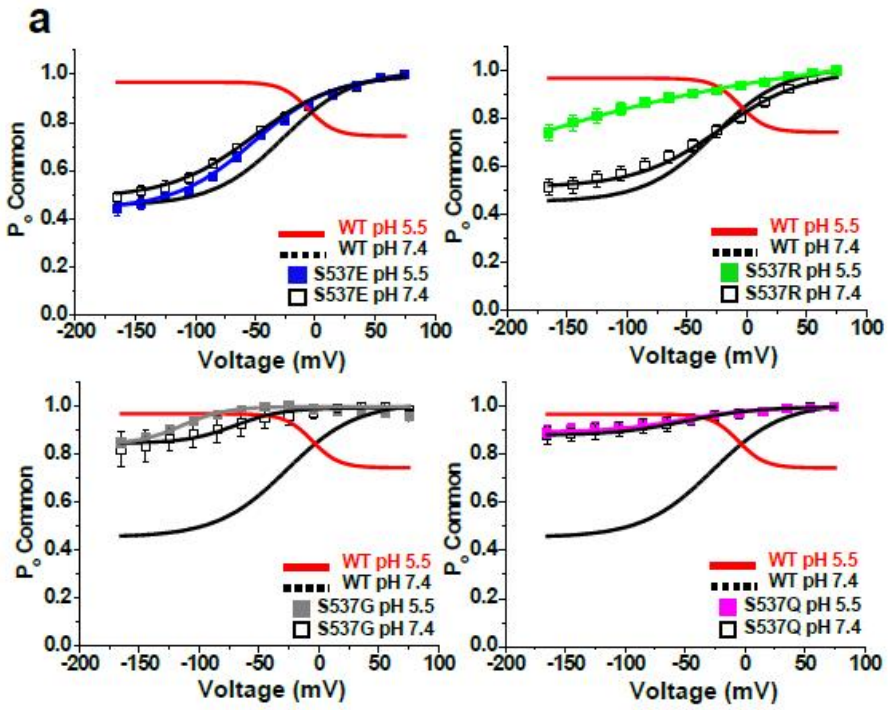
a
P_o Common
Voltage (mV)
WT pH 5.5
WT pH 7.4
S537E pH 5.5
S537E pH 7.4
S537R pH 5.5
S537R pH 7.4
S537G pH 5.5
S537G pH 7.4
S537Q pH 5.5
S537Q pH 7.4

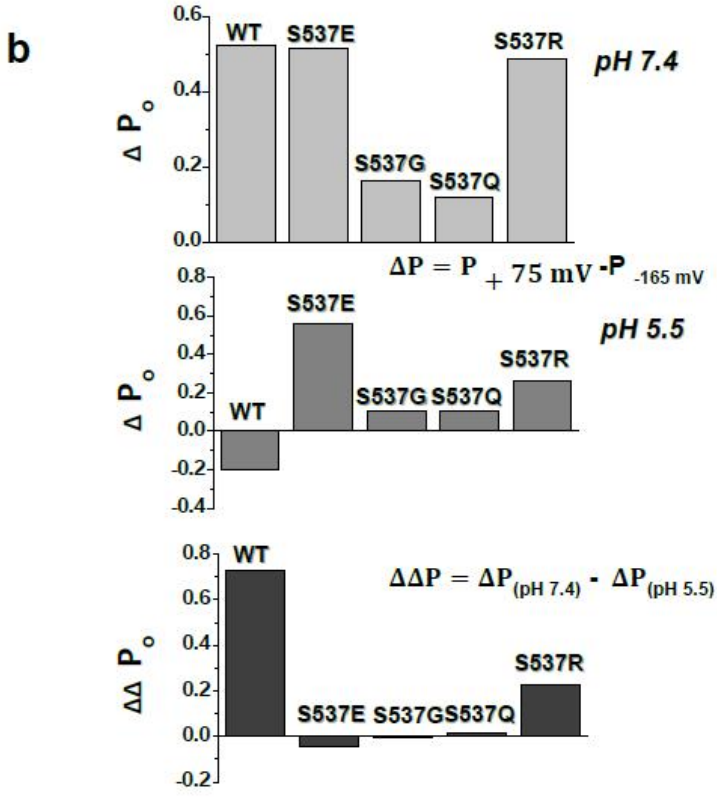
b
ΔP = P + 75 mV -P -165 mV
pH 7.4
pH 5.5
ΔΔP = ΔP(pH 7.4) - ΔP(pH 5.5)
ΔP_o
ΔΔP_o
WT
S537E
S537G
S537Q
S537R

Figure 9. Titratable residue at S537 plays a significant role in channel gating under pH variation.

a. The open probability curves of the common gate of S537 mutants under extracellular solutions of pH 7.4 and 5.5 conditions. Black dashed line and red line are the fits of equation indicating wild type ClC-1 at pH 7.4 and pH 5.5, respectively. Filled squares indicate the common gate open probability of the S537 mutants under bath solution of pH 5.5, and blanked ones under pH 7.4. n=3 (S537G pH 5.5, grey, S537Q pH 5.5, magenta), n=4 (S537E pH 5.5, blue) and n=6(S537R pH 5.5, green) Data are means ± s.e.m. **b.** Subtraction analysis of S537 mutants and wild type CLC-1. Bar graphs indicate parameters for measurement of changed voltage dependency of wild type CLC-1 and S537 mutants under bath solutions with different pH. The voltage dependency parameters were deduced using the equation $\Delta P = P_{+75mV} - P_{-165mV}$, where P_{+75mV} and P_{-165mV} are the open probabilities at +75 mV and -165 mV membrane potentials, respectively. **C.** $\Delta\Delta P$ was calculated by subtracting ΔP under bath solution of pH 5.5 from ΔP of pH 7.4. $\Delta\Delta P$ is the parameter applied to compare ΔP under pH 7.4 and pH 5 condition.

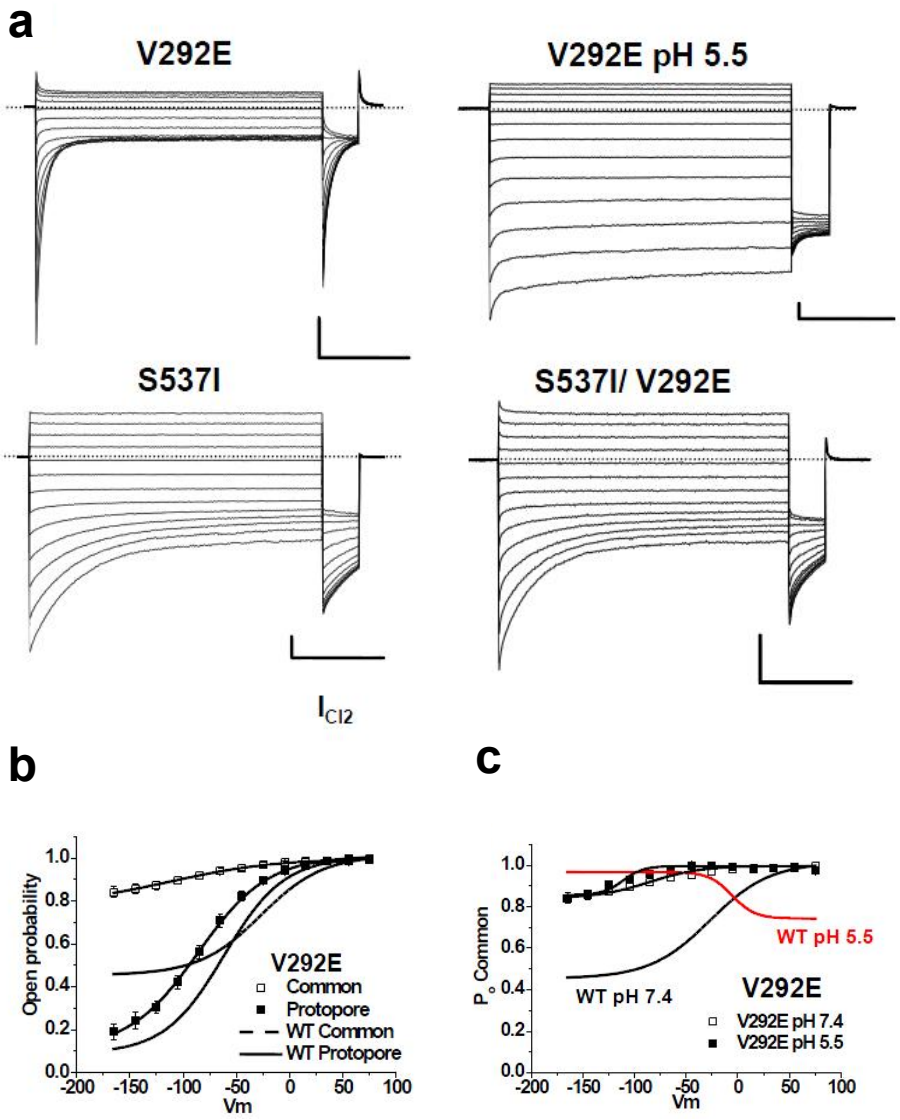

Figure 10. V292 and S537 mutants.

(a) Whole cell current traces of V292E, S537I, and V292E/S537I in extracellular pH 7.4 or pH 5.5. Dashed lines indicate zero current level. Scale bars represent 0.5 nA in vertical and 50 ms in horizontal. **(b)** Open probability of the protopore and common gate of V292E mutant. Filled squares indicate the protopore gate open probability, and blanked squares are for the open probability of the common gate of the V292E

mutant. Dashed and solid lines without data points indicate the open probability of the common gate and the protopore gate of the wild type hClC-1, respectively. **(c)** Open probabilities of the common gate of V292E mutant in bath solutions of pH 7.4 or 5.5. Filled squares and blanked squares indicate the open probabilities of the common gate of V292E under extracellular pH 5.5 and 7.4, respectively. Black dashed line and red line are the fits of equation (1), indicating the open probability of the common gate of wild type ClC-1 at pH 7.4 and pH 5.5, respectively. All data are expressed as means ± s.e.m. n=3 for V292E under bath solution of pH 5.5.

Table 2. Voltage dependent parameters of protopore and common gates from S537 mutants under different extracellular pH condition.

	$V_{1/2}$	*k*	P_{min}
common gating			
S537E	-50.77±6.7	44.9±6.1	0.49±0.02
S537R	1.17±8.4	53.7±9.4	0.60±0.10
S537G	-99.8±6.4	19.6±2.1	0.82±0.07
S537Q	-64.9±25.3	38.6±2.2	0.87±0.04
	$V_{1/2}$	*k*	P_{min}
common gating pH 5.5			
S537E	-50.12±4.8	38.2±4.5	0.44±0.03
S537R†	-	-	0.74±0.04
S537G†	-	-	0.85±0.01
S537Q†	-	-	0.89±0.03

	$V_{1/2}$	*k*	P_{min}
protopore gating			
S537E	-79.6±10.4	43.8±8.3	0.26±0.08
S537R	-56.2±14.3	77.4±24.2	0.36±0.05
S537G	-92.6±10.4	28.1±1.3	0.27±0.07
S537Q	-77.0±7.5	21.6±0.7	036.±0.05
	$V_{1/2}$	*k*	P_{min}
protopore gating pH 5.5			
S537E	-40.7±18.1	50.2±15.6	0.56±0.04
S537R†	-	-	0.91±0.04
S537G†	-	-	0.56±0.12
S537Q†	-	-	0.80±0.01

Data show the parameters obtained by fitting a Boltzmann equation to Voltage dependent data from each gate of S537 mutants. Data are means and s.e.m. † indicates the mutants that did not display voltage dependency.

5. Proton involvement is observed in hCLC-1 via S537.

Due to the modification of gating function of CLC-1 under low pH, the hypothesis suggested that proton influx is involved in the channel gating. G523X mutants showed the similar channel gating to wildtype CLC-1 under low pH, suggesting that G523D on helix O might display low intracellular pH level due to proton influx caused by open state conformation.

To investigate this hypothesis we examined pH titration for HEK293 overexpressing GFP-S65T tagged wildtype CLC-1, G523D, S537E, and double mutant, G523D and S537E that showed recovery of voltage dependency, respectively. It was previously reported that green fluorescent protein variants can be applied as a targeted pH sensor without indicator leakage and the toxicities of chemical indicators and invasive lading procedures (Keen *et al*., 1998; Hanson *et al*.,2002)

Figure 11 showed a measurement of intracellular pH modification by GFP-S65T tagged WT CLC-1, G523D, S537E, and double mutant, G523D and S537E, fluorescence. The control test that expressed GFP-S65T alone displayed the modification of fluorescence in response to addition and elimination of the weak acid acetate and base NH_4Cl (**Fig. 11**). WT CLC-1 GFP-S65T resulted in more changes in relative fluorescence compared to the control when adding the weak acid and slow reversible changes when subsequent perfusion was applied (**Fig. 11a,c**).

Thus, it is suggested that proton transport occurs in CLC-1 channel caused by a prompt acidification and slower alkalinization. However, G523D showed lower relative fluorescence compared to wildtype and the control, indicating that intracellular proton level is higher in the mutant before rapid acetic acid influx and dissociation

(**Fig. 11a, c**). Double mutant, S537E on G523D displayed the similar modification of fluorescence to wildtype CLC-1 in response to addition of the weak acid and removal of the weak base, which is consistent with the result of channel gating (**Fig. 11a, c**). S537E showed the similar kinetics of acidification to wildtype CLC-1, but rapid alkalinization, suggesting that S537E is involved in proton efflux mechanism (**Fig. 11a**).

Collectively, it was speculated that CLC-1 channel showed an aspect of exchanger and G523D and S537E on helix O are key modulators of proton involvement in CLC-1. However, it was impossible to detect the difference in the reversal potential in IV curve test when different pH extracellular solutions were applied. Thus, it cannot support the idea that proton transports across the CLC-1 channel (**Fig. 12**).

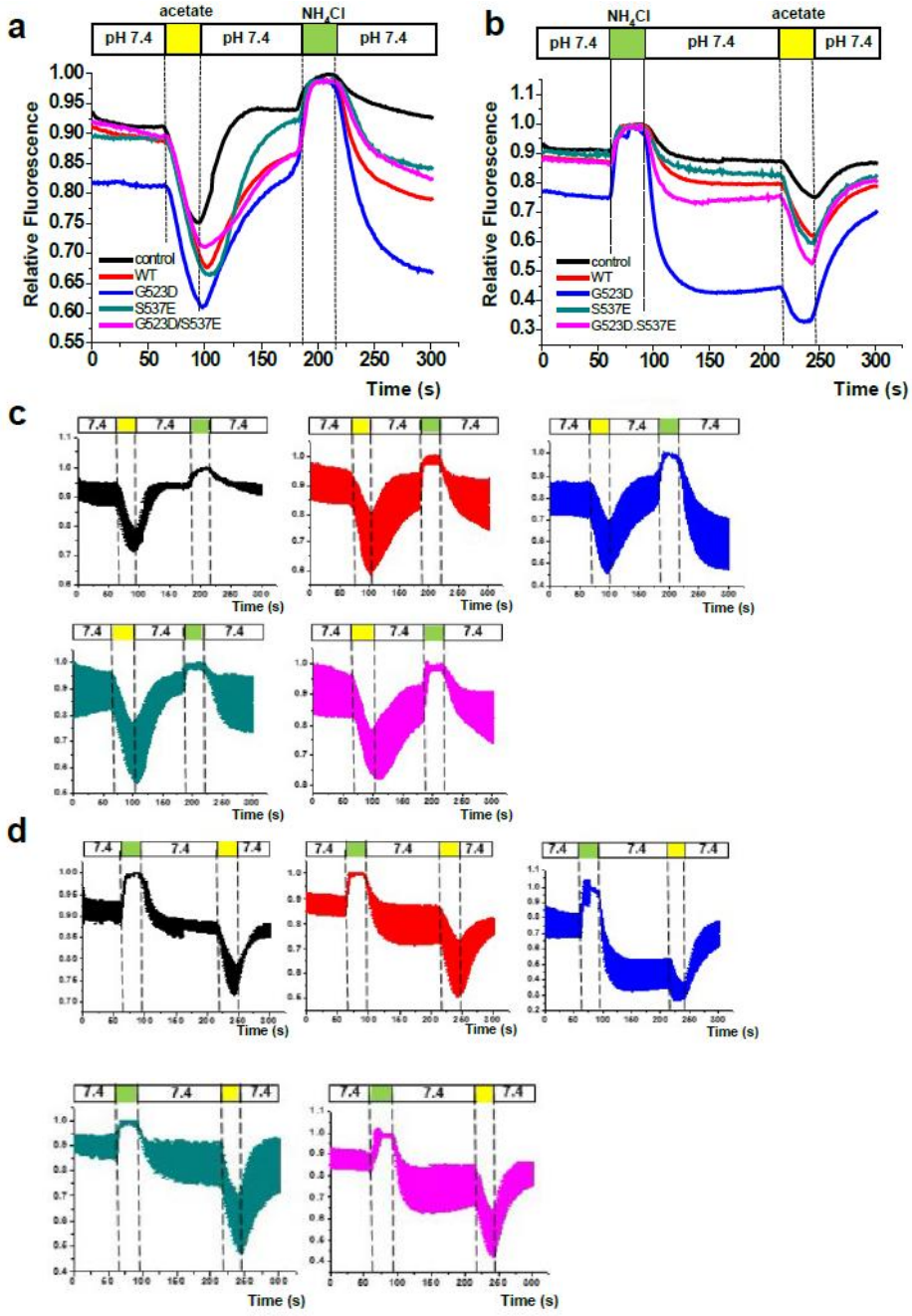
a
acetate
NH4Cl
pH 7.4
pH 7.4
pH 7.4
Relative Fluorescence
control
WT
G523D
S537E
G523D/S537E
Time (s)
b
NH4Cl
acetate
pH 7.4
pH 7.4
pH 7.4
Relative Fluorescence
control
WT
G523D
S537E
G523D.S537E
Time (s)
c
d
7.4
Time (s)

Figure 11. Time courses of pH changes in HEK cells by GFP-S65T fluorescence.

(a), (b) Comparison of the average of pH measurement in HEK 293 cells transiently expressing GFP-S65T as control (black), WT hCLC-1 (red), G523D (blue), S537E (green), and double mutant, G523D-S537E (magenta). The kinetics of fluorescence in response to addition of 30 mM sodium acetate and ammonium chloride were observed and vice versa. **(c), (d)** The measurement of pH changes in HEK 293 cells transiently expressing GFP-S65T, WT hCLC-1, G523D, S537E, and double mutant, G523D-S537E. Yellow and green box indicates the addition of 30 mM sodium acetate and 30 mM ammonium chloride. The average of relative fluorescence and error bars were indicated with thick line and thin line in the same color, respectively. n=7 (GFP-S65T), n=8 (WT), n=7 (G523D), n=10 (S537E), and n=9 (G523D-S537E). The reversed test was also conducted. n=5 (GFP-S65T), n=10 (WT), n=6 (G523D), n=9 (S537E), and n=5 (G523D-S537E). All data are means ± s.e.m.

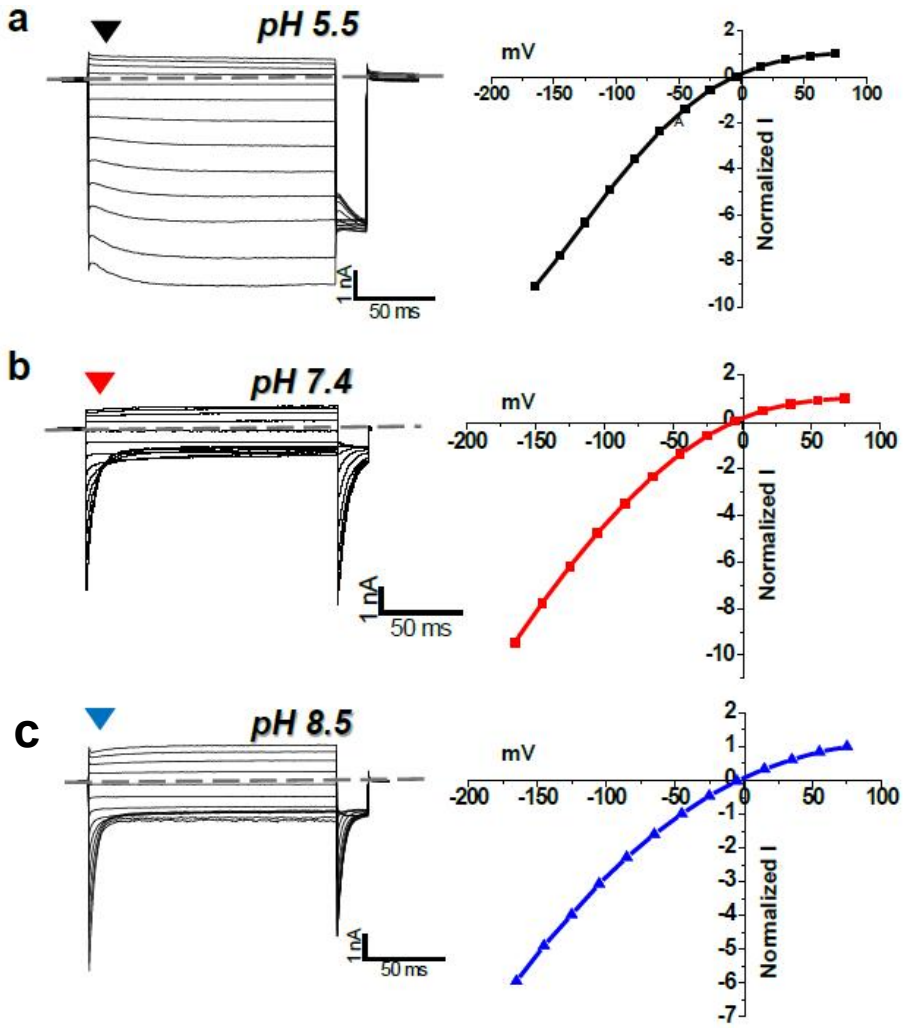

Figure 12. hCLC-1 reversal potential IV curve test.

(a),(b),(c) Electrophysiological characteristics of WT CLC-1 channel was measured in different pH extracellular solutions (pH 5.5, pH 7.4, and pH 8.5), and the IV curves were obtained where the arrow indicates.

6. CLC antiporter mimicking mutants, V292E and S537I, reveal an evolutionary key of CLC-1 to maintain its channel function

In CLC-ec1, I402 at the C-terminus of helix O interacts with the phenyl ring of Y_{cen} to occupy the central anion binding site (Basilio et al., 2014). The previous results suggested that S537 in CLC-1, corresponding to I402 in CLC-ec1, serves a key role in proton involvement as well as common gating, possibly interacting with Y_{cen} (Y578). E_{int} (E203) is known to be internal proton way-station in CLC-ec1 antiporter (Accardi et al., 2006), however, valine (V292) is placed in hCLC-1 instead of E_{int} (E203). According to Brett *et al* (Bennetts et al., 2013), V292 may push Y_{cen} during common gating process. Interestingly, V292E mutant displayed almost constitutively opened common gate, while the protopore gating is marginally affected (**Fig 10, Fig 13a**). It was previously shown that V292L also exhibits similar, almost opened common gating (Cederholm et al., 2010). Collectively, the results supported that V292 interacts with Y_{cen}, participating in the common gate.

Additionally, CLC antiporter-mimicking mutants were tested to find whether CLC-1 would still display channel function by substituting serine at 537 to isoleucine and valine at 292 to glutamate conserved in CLC-ec1. As mentioned earlier, V292E mutant produced constitutively opened common gate (**Fig. 10b, Fig. 13b**). The S537I mutant, mimicking the isoleucine of CLC-ec1 at the helix O, showed negatively shifted $V_{1/2}$ value and increased minimum open probability

(P_{min}) in the common gate (**Fig. 13c,d**). With the double mutation of S537I with V292E that mimics CLC-ec1, it was hypothesized that isoleucine at the C terminus of helix O may interact with Y_{cen} to play a major role in a common gate, and mutation of valine to glutamate (V292E) may affect CLC-1 channel function. Supporting this hypothesis, unlike V292E, the common gate of S537I/ V292E double mutant displays retained common gating (**Fig. 13b**). Rather, it resembles the open probability curve of S537I, and this supports the idea that the introduced isoleucine takes part in common gating even in the absence of V292. In addition, the $V_{1/2}$ value was compared with P_{min} among V292E, S537I and S537I/ V292E (**Fig. 13c**). P_{min} value of the double mutant was less than each single mutant, indicating that the double mutant retains common gating compared to other single mutants (**Fig. 13d**). All these data support the idea that substituted isoleucine can interact with Y_{cen}, as it is in CLC antiporters.

Taken together, it was hypothesized the structural conservation among these key 'Y_{cen}-interacting residues' play a key role in channel gating and structural stability to function as channel and C-terminus at helix O is closely involved in this process.

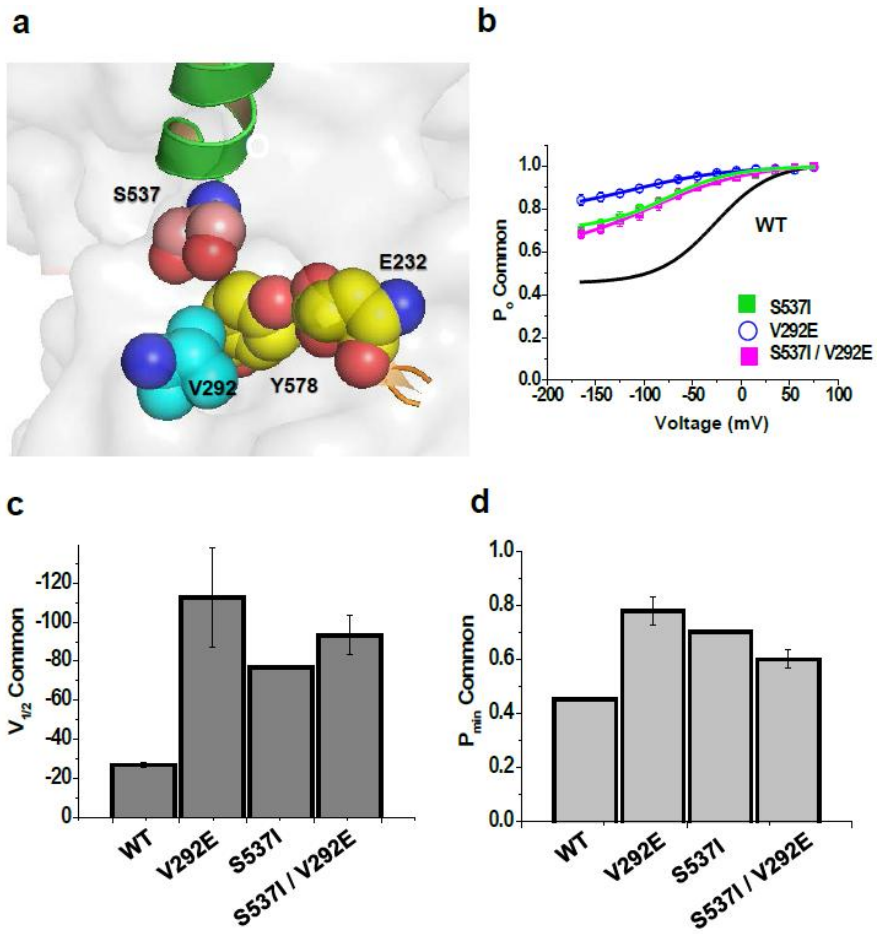

Figure 13. S537 is located in evolutionary remarkable site of CLC-1

a. Relative locations of residues S537, Y578 (Y_{cen}), E232 (E_{ext}), and V292 in CLC-1 homology model. Helix O was colored in green, and each residue is depicted as space-filled model and labeled S537 (pink), Y578 and E232 (yellow), and V292 (cyan). **b.** The open probabilities of

the common gate for mutants S537I, V292E, and double mutant S537I/V292E. Dashed line indicates the open probability of common gate of wild type ClC-1 fitted to the equation. n=4 (S537I and V292E) and n=3 (S537I/ V292E) **c.** The mean $V_{1/2}$ value of common gating curves of the wild type and the mutants with s.e.m. **d**. The bar graph indicates the minimum open probabilities of common gating obtained from wild type ClC-1 and the mutants. Data are means ± s.e.m.

7. A conserved salt bridge is crucial in gating function.

Highly conserved residues K231 and D136, as mutations of these residues induce hyperpolarization-activation characteristic of the channels (Fahlke *et al*., 1995; Fahlke *et al.*, 1997) are predicted to form salt bridges in CLC-1 (**Fig. 14**). In addition, the electrostatic linkage in the structures of CLC-ec1 and CLC-ecl E148Q was observed (**Fig. 14a**). Similar, but hydrophobic linkage was observed in the structure of a eukaryotic transporter cmCLC (**Fig. 4**). The structures of CLC-ec1 E148Q, CLC-ec1 wild type and cmCLC correspond to 'open protopore gate', 'closed protopore gate' and 'closed common gate' in CLC-1 each (Bennetts *et al*., 2013). In myotonic mutants D136G and K231A, salt bridge is reduced and those mutants are known to activate at hyperpolarizing potentials (Fahlke *et al*., 1995; Fahlke *et al*., 1997). Thus, the electrophysiological characteristics were obtained to find out charge reversal and charge swapping mutations, but channel currents in D136K mutant were only detected (**Fig. 14c**). K231D and double mutant D136K and K231D were non-functioning. D136K exhibits the traits of reversed voltage dependency in the common gate and constitutively opened fast gate. This linkage is important since it resides right next to E232 (**Fig. 15**), probably stabilizing helix F during CLC-1 gating. Taken together, it was concluded that salt bridge liking helix B and F is critical in maintaining normal voltage dependency of

CLC channels and is conserved throughout the CLC family.

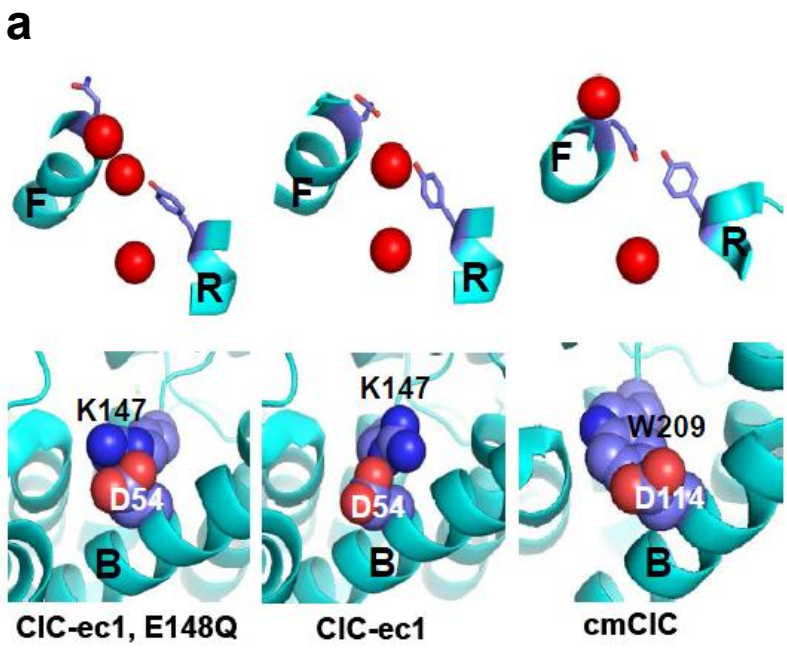

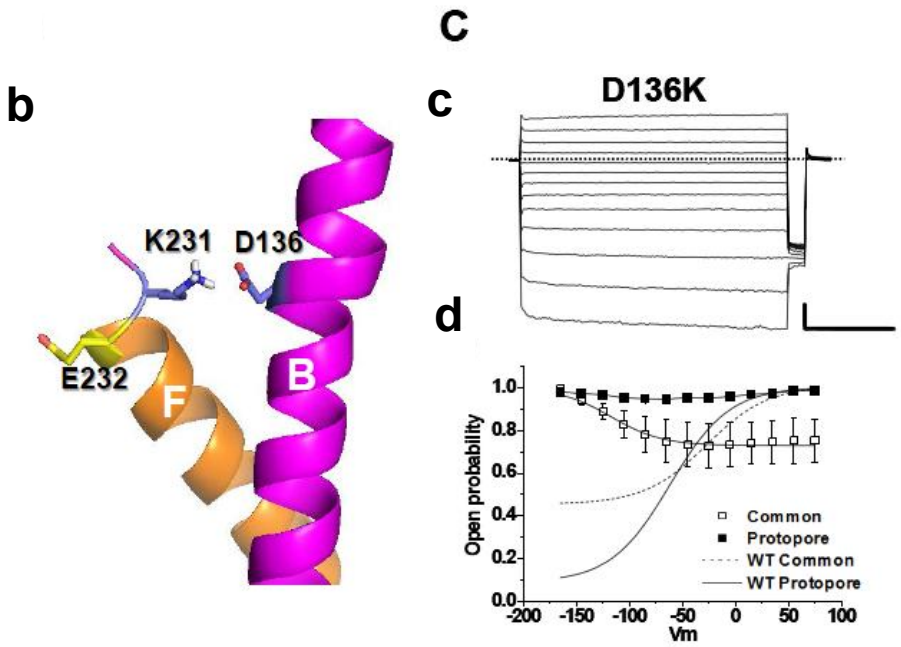

Figure 14. Salt bridge is a crucial determinant for the gating of CLC-1.

(a) Upper panels illustrate the gating states of ClC-ec1 mutant E148Q (PDB id; 1OTU, left), wild type ClC-ec1 (PDB id; 1OTS, middle), cmClC (PDB id; 3ORG, right). Corresponding interactions linking helices B and F are depicted in lower panels. Helices are depicted as ribbon in cyan. Space-filled spheres indicate the residues involved in the electrostatic or hydrophobic interaction between helices F and B.

(b) The ClC-1 molecular model suggests a salt bridge formed by K231 and D136 residues. Helices B (pink) and F (orange) are depicted as ribbons and selected residues, D136, K231, and E232 were drawn with sticks. **(c)** Whole cell current trace and open probability of common and

protopore gating in the D136K mutant. Dashed line in the whole cell trace indicates zero-current level and scale bars are 0.5 nA (vertical) and 50 ms (horizontal), respectively.

(d) The open probability of protopore gating (■) and common gating (□) were expressed as means ± s.e.m. . Dashed and solid lines without data points indicate the open probability of the common gate and the protopore gate of the wild type ClC-1, respectively. For D136K, n=3

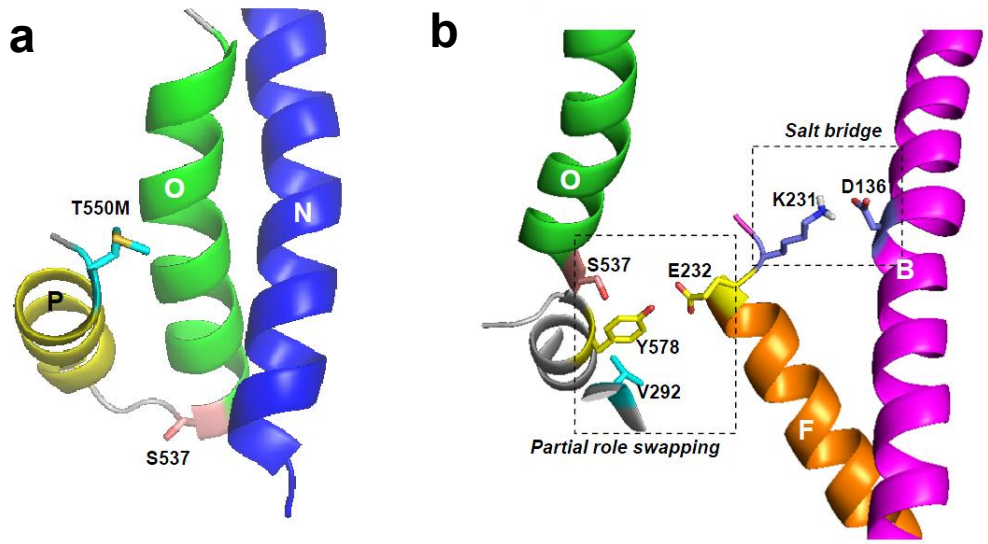

Figure 15. Location of the mutant sites and conserved structures in ClC-1 model.

(a) ClC-1 model showing location of T550M on helix P and potential interaction of this residue with S537 on helix O. Helix O (green), N (blue), and P (yellow) are depicted as ribbon and S537 (pink) and T550M (cyan) are shown as sticks. **(b)** Cartoon that illustrates the S537 (pink) on helix O (green) and nearby residues E232 (yellow), Y578 (yellow) and V292 (cyan). The salt bridge formed by the residues, K231 on helix F (orange) and D136 on helix B (magenta).

Discussion

The present study proposes that structural stability of helix O is a major contribution in the channel gating of CLC-1 channel. The data also suggest that S537 on helix O serves a role to maintain the conformational stability and is a significant contributor to distinct characteristic of the hyperpolarization-activated trait observed in the G523D mutant.

Similar to CLC antiporter, CLC channels does not only have the homodimeric architecture but also show gating kinetics modulated by the same residues; E_{ext} functions as a protopore gate and Y_{cen} works as a 'final effector' of the common gate (Bennetts *et al*., 2013). In addition, from structural design to gating mechanism, it is explicable that CLC proteins uniquely share multiple features.

For the CLC-1 proteins, the involvement of proton is a key determinant to mark a borderline between the antiporter and channel. It is suggested that S537 at C-terminus of helix O is deeply involved in the proton contribution. In addition, S537 at the C-terminal of the helix O was previously reported as an inhibitor binding pocket (Estevez *et al*., 2003) where hydrophobic inhibitor 9-AC can bind to the intracellular side of the channel. In CLC-ec1, the corresponding isoleucine locates at the C-terminal of helix O and is known to interact with Y_{cen} to function as an inner gate (Bennetts *et al*., 2013). Similar to its role in CLC-ec1, S537 in CLC-1 is also important in the common gating (**Fig. 7,9**) and may interact with Y_{cen}. Furthermore, it is also hypothesized that S537 and V292 are essential components to interact with Y_{cen} (**Fig. 13**), thereby modulating normal channel function. These data support the idea that the Y_{cen}-pushing role of I402 in CLC-ecl is replaced by S537 and V292 in the CLC-1 channel. V292 corresponds to E_{int} that is critical for transport mechanism of proton in antiporter-type CLC

proteins. As V292 lost its role in proton transport in the CLC-1 channel, it is tentatively proposed that S537 is a remarkable site that determines a difference between the channel and aniporter. (**Fig. 13**). It is speculated that this 'partial role swap' of S537 and V292 is a key evolutionary step for CLC-1 to act as channel. Eukaryotic CLC antiporter cmCLC also lacks E_{int}, but it is replaced by threonine at the corresponding position. At the C-terminal of helix O of cmCLC also lies threonine, probably hinting that cmCLC represents an intermediate form in transition state to CLC channels.

By investigating myotonic mutants with novel characteristic of activating at hyperpolarizing membrane potential, some important amino acid residues were identified. Supporting this idea, mutations of the aspartic acid residue in some CLC proteins, corresponding to D136 in CLC-1, result in malfunctioning or alteration in electrochemical feature of proteins (Barvencik *et al*., 2014; De Stefano *et al*., 2013; Picollo *et al*., 2004). T550 is another highly conserved residue and it resides on the extracellular surface of the helix P (**Fig. 4**). The mutants that activates upon hyperpolarized potentials can be significant in clinical aspect. The modified voltage dependency of the mutant results in minimum P_o value at voltages positive to the $E_{cl,}$ thereby causing inward rectification of the mutant channel with cell Cl^- efflux, but avoid Cl^- influx. Therefore, the action potentials fired during muscle

excitement can lead to intracellular Cl^- depletion and eventually shift the E_{cl} to negative potentials. Thus, g_{cl} would not function at the resting membrane potential (Fahlke *et al.*, 1995). G523D displays similar channel kinetics as D136G which was previously reported as myotonic mutant and it is plausible that G523D may play a role in $g_{cl,}$ which is not effective at the resting membrane potential. The location of these mutants also indicate the significance of helix O. Helix P is directly connected to C-terminus of helix O and is located at the dimer interface. Thus, helix O together with helices N and P may account for the voltage dependency of the CLC channel. Interestingly, all these hyperpolarization-activated mutation sites are located at the extracellular surface of the channel (**Fig. 4**). Mutations at the extracellular side of the channel induce structural modifications, thereby possibly change the arrangement of the central anion binding site including Y_{cen}. This may infer that normal voltage dependency or voltage sensing of the CLC-1 is largely related to the extracellular side of the channel.

In summary, the data assess the importance of helix O as the main contributor for stable structure of evolutionary conserved CLC proteins. The structural modification of helix O caused by mutations at C-terminus and N-terminus plays a key role in voltage dependency in CLC-1. The role of pushing Y_{cen} to function as common gate is

replaced by S537 and V292 in the channel, but proton transport is not mediated due to untitratable site around S537 (**Fig. 16**). However, it is possible that S537 serves a role in stabilizing central anion binding site through noncovalent interaction, especially hydrogen bonding. It was previously suggested by *Bennetts et al., 2013* that lower half of the helices including helices G, I, O, H, and R is engaged in the common gating, and the results suggested proton affects the channel gate via S537 on helix O, modulating the conformational arrangement in CLC-1.

Collectively, these results indicate that the structure with respect to chloride gating is evolutionarily conserved and the distinct characteristics between antiporter and channel. It is suggested that 'partial role swap model' is a pivotal step in transitioning from antiporters to channels, and proposed that S537 on helix O is the remarkable site in channel gating, where proton can possibly involve in the CLC-1channel function.

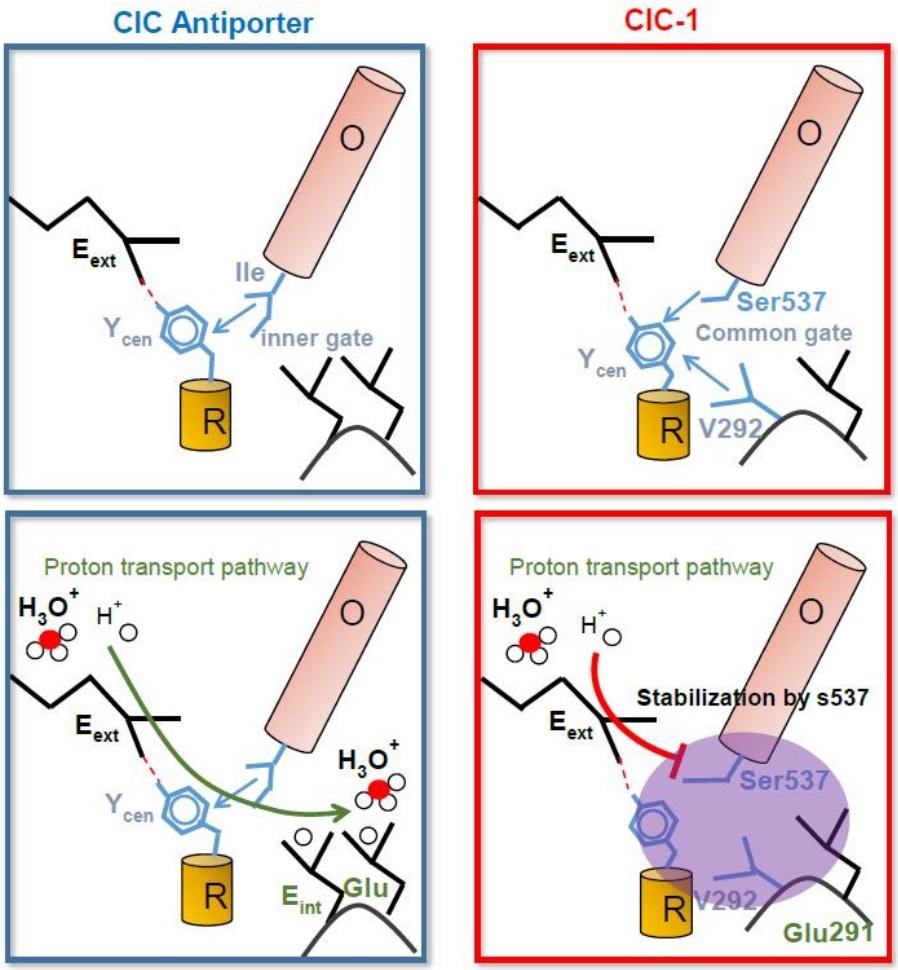

Figure 16. 'Partial role swap' model in evolution of the ClC-1.

Illustrations of chloride gating mechanism and a possible proton pathway in ClC proteins. Cartoons in the blue and green box show inner gating and common gating mechanism in ClC antiporter and ClC-1, respectively. Cartoons in the bottom indicate proton pathway in ClC antiporter and possible proton pathway in ClC-1. Residues colored in blue are assumed to be engaged in the inner gate or common gate in ClC antiporter or ClC-1, respectively. Residues in green are suggested to be important in the proton transport. Red dotted lines in the blue boxes indicate hydrogen bonding between E_{ext} and Y_{cen}.

REFERENCES

1. Accardi A. Structure and gating of CLC channels and exchangers. J Physiol. 2015 **593**(18): 4129–4138.

2. Accardi A, Lobet S, Williams S, Miller C, and Dutzler R. Synergism between halide binding and proton transport in a CLC-type exchanger. J Mol Biol 2006 **362**(4): 691–699.

3. Accardi A, and Miller C. Secondary active transport mediated by a prokaryotic homologue of ClC Cl- channels. Nature. 2004 **427**(6977): 803–807.

4. Accardi A, and Pusch M. Fast and slow gating relaxations in the muscle chloride channel CLC-1. J Gen Physiol 2000 **116**(3): 433–444.

5. Accardi, A, Walden M, Nguitragool W, Jayaram H, Williams C, and Miller C. Separate ion pathways in a Cl-/H+ exchanger. J Gen Physiol 2005 **126**(6): 563–570.

6. Barvencik F, Kurth I, Koehne T, Stauber T, Zustin J, Tsiakas K, *et al*. CLCN7 and TCIRG1 mutations differentially affect bone matrix mineralization in osteopetrotic individuals. J Bone Miner Res 2014 **29**(4): 982–991.

7. Basilio D, Noack K, Picollo A and Accardi A. Conformational changes required for H(+)/Cl(-) exchange mediated by a CLC transporter. Nat Struct Mol Biol 2014 **21**(5): 456–463.

8. Bennetts B, and Parker MW. Molecular determinants of common gating of a ClC chloride channel. 2013 Nat Commun **4**: 2507.

9. Bennetts B, Parker MW, and Cromer BA. Inhibition of skeletal muscle ClC-1 chloride channels by low intracellular pH and ATP. J Biol Chem 2007 **282**(45): 32780-32791.

10. Bisset D, CorryB, and Chung SH. The fast gating mechanism in ClC-0 channels. 2005 Biophys J **89**(1): 179-186.

11. Blanz J, Schweizer M, Auberson M, Maier H, Muenscher A, Hubner CA et al., Leukoencephalopathy upon disruption of the chloride channel ClC-2. J Neurosci 2007 **27**(24): 6581-6589.

12. Bosl MR, Stein V, Hubner C, Zdebik AA, Jordt SE, Mukhopadhyay AK, *et al*. Male germ cells and photoreceptors, both dependent on close cell-cell interactions, degenerate upon ClC-2 Cl(-) channel disruption. EMBO J 2001 **20**(6): 1289-1299.

13. Bretag A, Antimyotic agents and myotonia. Proc Aust Physiol Pharmacol Soc 1983 (67):618-724

14. Cederholm JM, Rychkov GY, Bagley CJ, and Bretag AH Inter-subunit communication and fast gate integrity are important for common gating in hClC-1. Int J Biochem Cell Biol 2010 **42**(7): 1182-1188.

15. Cheng MH, Mamonov AB, Dukes JW, and Coalson RD Modeling the fast gating mechanism in the ClC-0 chloride channel. J Phys Chem B 2007 **111**(21): 5956-5965.

16. De Santiago JA, Nehke K, Arreola J. Quantitative analysis of the voltage-dependent gating of mouse parotid CLC-2 chloride channel. J Gen Physiol 2005 **126**(6):591-603

17. De Stefano S, Pusch M, and Zifarelli G. A single point mutation reveals gating of the human ClC-5 Cl-/H+ antiporter. J Physiol 2013 **591**(23): 5879-5893.

18. Duan D, Winter C, Cowley S, Hume JR and Horowitz B Molecular identification of a volume-regulated chloride channel. Nature. 1997 **390**(6658): 417-421.

19. Duffield M, Rychkov G, Bretag A, and Roberts M. Involvement of helices at the dimer interface in ClC-1 common gating. J Gen Physiol 2003 **121**(2): 149-161.

20. Dutzler R, Campbell EB, Cadene M, Chait BT and MacKinnon R. X-ray structure of a ClC chloride channel at 3.0 A reveals the molecular basis of anion selectivity. Nature. 2002 **415**(6869): 287-294.

21. Dutzler R, Campbell EB, and MacKinnon R Gating the selectivity filter in ClC chloride channels. Science 2003 **300**(5616): 108-112.

22. Engh AM, and Maduke M. Cysteine accessibility in ClC-0 supports conservation of the ClC intracellular vestibule. J Gen Physiol 2005 **125**(6): 601-617.

23. Estevez R, Boettger T, Stein V, Birkenhager R, Otto E, Hildebrandt F et al. Barttin is a Cl^- channel beta-subunit crucial for renal Cl^- reabsorption and

inner ear K^+ secretion. Nature 2001 **414**(6863): 558-561.

24. Estevez R, Schroeder BC, Accardi A, Jentsch TJ and Pusch M. Conservation of chloride channel structure revealed by an inhibitor binding site in ClC-1. Neuron 2003 **38**(1): 47-59.

25. Fahlke C, Rhodes TH, Desai RR and George, Jr AL. Pore stoichiometry of a voltage-gated chloride channel. Nature. 1998 **394**(6694): 687-690.

26. Fahlke C, Rudel R, Mitrovic N, Zhou M and George Jr AL. An aspartic acid residue important for voltage-dependent gating of human muscle chloride channels. Neuron. 1995 **15**(2): 463-472.

27. Fahlke C, Yu HT, Beck CL, Rhodes TH, and George Jr AL. Pore-forming segments in voltage-gated chloride channels. Nature. 1997 **390**(6659): 529-532.

28. Feng L, Campbell EB, Hsiung Y and MacKinnon R Structure of a eukaryotic CLC transporter defines an intermediate state in the transport cycle. Science. 2010 **330**(6004): 635-641.

29. Feng L, Campbell EB, and MacKinnon R. Molecular mechanism of proton transport in CLC Cl^-/H^+ exchange transporters. Proc Natl Acad Sci U S A. 2012 **109**(29): 11699-11704.

30. Frattini A, Pangrazio A, Susani L, Sobacchi C, Mirolo M, Abinun M, et al. Chloride channel ClCN7 mutations are responsible for severe recessive, dominant, and intermediate osteopetrosis. J Bone Miner Res. 2003 **18**(10): 1740-1747.

31. Gurnett CA, Kahl SD, Anderson RD, Campbell KP. Absence of the skeletal muscle sarcolemma chloride channel CLC-1 in myotonic mice. J Biol Chem. 1996 **270**(16):9035-9038

32. Ha K, Kim SY, Hong C, Myeong J, Shin JH, Kim DS, et al. Electrophysiological characteristics of six mutations in hClC-1 of Korean patients with myotonia congenita. Mol Cells 2014 **37**(3): 202-212.

33. Han W, Cheng RC, Maduke MC and Tajkhorshid E. Water access points and hydration pathways in CLC H+/Cl- transporters. Proc Natl Acad Sci U S A. 2014 **111**(5): 1819-1824.

34. Hanson GT, McAnaney TB, Park ES, Rendell ME, Yarbrough DK, Chu S, Xi L, Boxer SG, Montrose MH, Remington SJ. Green Fluorescenct protein variants as ratiometric dual emission pH sensors. I. Structural characteristics and preliminary application. Biochemistry 2000 **41**(52):1477-15488

35. Hayama A, Rai T, Sasaki S, and Uchida S. Molecular mechanisms of Bartter syndrome caused by mutations in the BSND gene. Histochem Cell Biol. 2003 **119**(6): 485-493.

36. Hille B. Axons, ions, and dons. Science. 1992 **258**(5079): 144-145.

37. Imbrici P, Altamura C, Pessia M, Mantegazza R, Desaphy JF and Camerino DC ClC-1 chloride channels: state-of-the-art research and future challenges. Front Cell Neurosci. 2015 **9**: 156.

38. Jentsch, T. J. (2008). "CLC chloride channels and transporters: from genes to protein structure, pathology and physiology." Crit Rev Biochem Mol Biol **43**(1): 3-36.

39. Jentsch TJ, Gunther W, Pusch M and Schwappach B. Properties of voltage-gated chloride channels of the ClC gene family. J Physiol. 1995 **482**: 19S-25S.

40. Jentsch TJ, Neagoe I, and Scheel O. CLC chloride channels and transporters. Curr Opin Neurobiol. 2005 **15**(3): 319-325.

41. Jentsch TJ, Steinmeyer K, and Schwarz G. Primary structure of Torpedo marmorata chloride channel isolated by expression cloning in Xenopus oocytes." Nature. 1990 **348**(6301): 510-514.

42. Kazachenko VN, Kochetkov KV, Aslanidi OV and Grinevich AA Study of fractal properties of single ionic channel gating mechanism by the fast Fourier transform. Biofizika 2001 **46**(6): 1062-1070.

43. Kneen M, Farinas J, Li Y, Verkman AS. Green fluorescent protein as a noninvasive intracellular pH indicator. Biophy J. 1998 **74**(3):1591-1599

44. Kobayashi K, Uchida S, Mizutani. S, Sasaki S and Marumo F. Developmental expression of CLC-K1 in the postnatal rat kidney. Histochem Cell Biol. 2001 **116**(1): 49-56.

45. Kornak U, Kasper D, Bosl MR, Kaiser E, Schweizer M, Schulz A, et al. Loss of the ClC-7 chloride channel leads to osteopetrosis in mice and man. Cell. 2001 **104**(2): 205-215.

46. Lim HH, and Miller C. Intracellular proton-transfer

mutants in a CLC Cl^-/H^+ exchanger. J Gen Physiol. 2009 **133**(2): 131-138.

47. Lim HH, Shane T, and Miller C. Intracellular proton access in a Cl^-/H^+ antiporter. PLoS Biol. 2012 **10**(12): e1001441.

48. Lin CW, and Chen TY. Probing the pore of ClC-0 by substituted cysteine accessibility method using methane thiosulfonate reagents. J Gen Physiol. 2003 **122**(2): 147-159.

49. Lisal J, and Maduke M. The ClC-0 chloride channel is a 'broken' Cl^-/H^+ antiporter. Nat Struct Mol Biol. 2008 **15**(8): 805-810.

50. Lisal J. and Maduke M. Review. Proton-coupled gating in chloride channels. Philos Trans R Soc Lond B Biol Sci. 2009 **364**(1514): 181-187.

51. Ludewig U, Pusch M and Jentsch TJ. Two physically distinct pores in the dimeric ClC-0 chloride channel. Nature. 1996 **383**(6598): 340-343.

52. Ma L, Rychkov GY, Bykova EA, Zheng J and Bretag AH. Movement of hClC-1 C-termini during common gating and limits on their cytoplasmic location. Biochem J. 2011 **436**(2): 415-428.

53. Matsumura Y, Uchida S, Kondo Y, Miyazaki H, Ko SB, Hayama A, et al. Overt nephrogenic diabetes insipidus in mice lacking the CLC-K1 chloride channel. Nat Genet. 1999 **21**(1): 95-98.

54. Middleton RE, Pheasant DJ, and Miller C Homodimeric architecture of a ClC-type chloride ion channel. Nature. 1996 **383**(6598): 337-340.

55. Miller C. Open-state substructure of single chloride channels from Torpedo electroplax. Philos Trans R Soc Lond B Biol Sci. 1982 **299**(1097): 401-411.

56. Miller C. ClC chloride channels viewed through a transporter lens. Nature. 2006 **440**(7083): 484-489.

57. Miller C, and Nguitragool W. A provisional transport mechanism for a chloride channel-type Cl-/H+ exchanger. Philos Trans R Soc Lond B Biol Sci. 2009 **364**(1514): 175-180.

58. Miller FJ, Filali M, Huss GJ, Stanic B, Chamseddine A, Barna TJ, et al Cytokine activation of nuclear factor kappa B in vascular smooth muscle cells requires signaling endosomes containing Nox1 and ClC-3. Circ Res. 2007 **101**(7): 663-671.

59. Nehrke K, Arreola J, Nguyen HV, Pilato J, Richardson L, Okunade G, Baggs R, et al. Loss of hyperpolarization-activated Cl^- current in salivary acinar cells from Clcn2 knockout mice. J Biol Chem. 2002 **277**(26): 23604-23611.

60. Nguitragool W, and Miller C. CLC Cl^-/H^+ transporters constrained by covalent cross-linking. Proc Natl Acad Sci U S A. 2007 **104**(52): 20659-20665.

61. Papponen H, Kaisto T, Myllyla VV, Myllyla R, Metsikko K. Regulated sarcolemmal localization of the muscle-specific CLC-1 chloride channel. Exp Neurol. 2005 **191**(1):163-173

62. Park E, Earnest B, MacKinnon C, MacKinnon R.

Structure of a CLC chloride ion channel by cryo-electron microscopy. Nature 2016[epub ahead of print]

63. Picollo A, Liantonio A, Didonna MP, Elia L, Camerino DC, and Pusch M. Molecular determinants of differential pore blocking of kidney CLC-K chloride channels. EMBO Rep 2004 **5**(6): 584-589.

64. Picollo A, and Pusch M. Chloride/proton antiporter activity of mammalian CLC proteins ClC-4 and ClC-5. Nature. 2005 **436**(7049): 420-423.

65. Piwon N, Gunther W, Schwake M, Bosl MR, and Jentsch TJ. ClC-5 Cl^- channel disruption impairs endocytosis in a mouse model for Dent's disease. Nature. 2000 **408**(6810): 369-373.

66. Poet M, Kornak U, Schweizer M, Zdebik AA, Scheel O, Hoelter S, Wurst W, et al. Lysosomal storage disease upon disruption of the neuronal chloride transport protein ClC-6. Proc Natl Acad Sci U S A. 2006**103**(37): 13854-13859.

67. Pusch M. Myotonia caused by mutations in the muscle chloride channel gene CLCN1. Hum Mutat. 2002 **19**(4): 423-434.

68. Pusch M. Structural insights into chloride and proton-mediated gating of CLC chloride channels. Biochemistry. 2004 **43**(5): 1135-1144.

69. Pusch M, Ludewig U, Rehfeldt A and Jentsch TJ Gating of the voltage-dependent chloride channel CIC-0 by the permeant anion. Nature. 1995 **373**(6514): 527-531.

70. Ryan A, Rudel R, Kuchenbecker M, and Fahlke C. A

novel alteration of muscle chloride channel gating in myotonia levior. J Physiol. 2002 **545**(Pt 2): 345-354.

71. Rychkov GY, Pusch M, Astill DS, Roberts ML, Jentsch TJ, and Bretag AH. Concentration and pH dependence of skeletal muscle chloride channel ClC-1. J Physiol. 1996 **497 (Pt 2)**: 423-435.

72. Salazar G, Love R, Styers ML, Werner E, Peden A, Rodriguez S, Gearing M, et al. AP-3-dependent mechanisms control the targeting of a chloride channel (ClC-3) in neuronal and non-neuronal cells." J Biol Chem. 2004 **279**(24): 25430-25439.

73. Sali A, and Blundell TL. Comparative protein modelling by satisfaction of spatial restraints. J Mol Biol. 1993 **234**(3): 779-815.

74. Scheel O, Zdebik AA, Lourdel S, and Jentsch TJ. Voltage-dependent electrogenic chloride/proton exchange by endosomal CLC proteins. Nature. 2005 **436**(7049): 424-427.

75. Scholl U, Hebeisen S, Janssen AG, Muller G, Newen G, Alekov A, et al. Barttin modulates trafficking and function of ClC-K channels. Proc Natl Acad Sci U S A. 2006 **103**(30): 11411-11416.

76. Simon DB, Bindra RS, Mansfield TA, Nelson-Williams C, Mendonca E, et al. Mutations in the chloride channel gene, CLCNKB, cause Bartter's syndrome type III. Nat Genet. 1997 **17**(2): 171-178.

77. Steinmeyer K, Klocke R, Ortland C, Gronemeier M, Jockusch H, et al. Inactivation of muscle chloride channel by transposon insertion in myotonic mice.

Nature. 1991 **354**(6351): 304-308.

78. Steinmeyer K, Lorenz C, Pusch M, Koch MC, and Jentsch TJ. Multimeric structure of ClC-1 chloride channel revealed by mutations in dominant myotonia congenita (Thomsen). EMBO J. 1994 **13**(4): 737-743.

79. Steinmeyer K, Schwappach B, Bens M, Vandewalle A, and Jentsch TJ. Cloning and functional expression of rat CLC-5, a chloride channel related to kidney disease. J Biol Chem. 1995 **270**(52): 31172-31177.

80. Steinmeyer K, Ortland C, Jentsch TJ. Primary structure and functional expression of a developmentally regulated skeletal muscle chloride channel. Nature 1991 **354**(6351):301-304

81. Stobrawa SM, Breiderhoff T, Takamori S, Engel D, Schweizer M, Zdebik AA, et al. Disruption of ClC-3, a chloride channel expressed on synaptic vesicles, leads to a loss of the hippocampus. Neuron. 2001 **29**(1): 185-196.

82. Stolting G, Fischer M, and Fahlke C. CLC channel function and dysfunction in health and disease. Front Physiol. 2014 **5**: 378.

83. Stolting G, Fischer M, and Fahlke C. CLC-1 and CLC-2 form hetero-dimeric channels with novel protopore functions. Pflugers Arch **466**(12):2191-2804

84. Tamura K, Stecher G, Peterson D, Filipski A, and Kumar S. MEGA6: Molecular Evolutionary Genetics Analysis version 6.0." Mol Biol Evol. 2013 **30**(12): 2725-2729.

85. Tang CY, and Chen TY. Physiology and pathophysiology of CLC-1: mechanisms of a chloride channel disease, myotonia. J Biomed Biotechnol 2011: 685328.

86. Thiemann A, Grunder S, Pusch M, and Jentsch TJ. A chloride channel widely expressed in epithelial and non-epithelial cells. Nature. 1992 **356**(6364): 57-60.

87. Uchida S, Sasaki S, Nitta K, Uchida K, Horita S, Nihei H and Marumo F. Localization and functional characterization of rat kidney-specific chloride channel, ClC-K1. J Clin Invest. 1995 **95**(1): 104-113.

88. Vandewalle A, Cluzeaud F, Bens M, Kieferle S, Steinmeyer K, and Jentsch TJ. Localization and induction by dehydration of ClC-K chloride channels in the rat kidney. Am J Physiol. 1997 **272**(5 Pt 2): F678-688.

89. Vandewalle A, Cluzeaud F, Peng KC, Bens M, Luchow A, et al. Tissue distribution and subcellular localization of the ClC-5 chloride channel in rat intestinal cells. Am J Physiol Cell Physiol. 2001 **280**(2): C373-381.

90. Waguespack SG, Hui SL, Dimeglio LA and Econs MJ. Autosomal dominant osteopetrosis: clinical severity and natural history of 94 subjects with a chloride channel 7 gene mutation. J Clin Endocrinol Metab. 2007 **92**(3): 771-778.

91. Waguespack SG, Koller DL, White KE, Fishburn T, Carn G, Buckwalter KA, et al. Chloride channel 7 (ClCN7) gene mutations and autosomal dominant

osteopetrosis, type II. J Bone Miner Res. 2003 **18**(8): 1513-1518.

92. Waldegger S, Jeck N, Barth P, Peters M, Vitzthum H, Wolf K, et al. Barttin increases surface expression and changes current properties of ClC-K channels." Pflugers Arch. 2002 **444**(3): 411-418.

93. Waldegger S, and Jentsch TJ. Functional and structural analysis of ClC-K chloride channels involved in renal disease. J Biol Chem. 2000 **275**(32): 24527-24533.

94. Walden M, Accardi A, Wu F, Xu C, Williams C, and Miller C. Uncoupling and turnover in a Cl^-/H^+ exchange transporter. J Gen Physiol. 2007 **129**(4): 317-329.

95. Wang XQ, Deriy LV, Foss S, Huang P, Lamb FS, Kaetzel MA, et al. CLC-3 channels modulate excitatory synaptic transmission in hippocampal neurons. Neuron. 2006 **52**(2): 321-333.

96. Weinreich F, and Jentsch TJ. Pores formed by single subunits in mixed dimers of different CLC chloride channels. J Biol Chem. 2001 **276**(4): 2347-2353.

97. Weiss DS, and Magleby KL. Voltage-dependent gating mechanism for single fast chloride channels from rat skeletal muscle. J Physiol. 1992 **453**: 279-306.

98. Wrong OM, Norden AG, and Feest TG. Dent's disease; a familial proximal renal tubular syndrome with low-molecular-weight proteinuria, hypercalciuria, nephrocalcinosis, metabolic bone disease, progressive renal failure and a marked

male predominance. QJM. 1994 **87**(8): 473-493.

99. Wu FF, Ryan A, Devaney J, Warnstedt M, Korade-Mirnics Z, Poser B, et al. Novel CLCN1 mutations with unique clinical and electrophysiological consequences. Brain. 2002 **125**(Pt 11): 2392-2407.

100. Zhang J, Sanguinetti MC, Kwiecinski H, and LJ Ptacek. Mechanism of inverted activation of ClC-1 channels caused by a novel myotonia congenita mutation. J Biol Chem. 2000 **275**(4): 2999-3005.

국문 초록

우리 몸에서 가장 풍부한 음이온인 Cl^- 이온통로들은 많은 조직에 분포하며 다양한 생리학적인 역할을 수행한다. 그 중 CLC family 는 고전적인 의미의 channel 들 뿐만 아니라 Cl^-/H^+exchanger 로 작동하는 종류들도 포함하고 있다. 그 역할과 작동기전이 다름에도 불구하고 CLC family 의 channel 과 exchanger 들은 매우 유사한 double barreled structure 를 가지고 있다. 그 중 CLC-1 은 막전압 탈분극시 더 활성화되는 Voltage-gated chloride channel 이다. CLC-1 은 골격근에 집중적으로 분포하며 활동전압의 신속한 재분극에 중요하다. CLC-1 의 돌연변이는 선천성 근육긴장증 등을 유발한다. CLC-1 의 작동기전, 즉 이온통로 개폐 (gating) 기전으로는 double barrel 구조인 두 통로를 독립적으로 조절하는 protopore gating 뿐만 아니라 두 통로를 함께 조절하는 common gating 이 작동한다. 이 논문에서는 선천성 근육긴장증 환자에서 발견된 돌연변이들 중, common gating 의 전압의존성이 반대방향으로 보이는 G523D 를 조사하였다. 특히 CLC-1 의 전체 구조 중 helix O 의 C-terminal 쪽 아미노산 S537 에 주목하였다. 3 차원 구조에서 유추할 때, 이 잔기가 channel 과 exchanger 의 특성을 결정짓는 구조 단위로 제시되었기 때문이다.

G523D CLC-1 의 S537 을 pH-titratable 아미노산인 Glu 로 치환하면 정상적인 common gating 으로 회복되었다. Wild type

CLC-1 에서 S537 을 다양하게 치환해 보니, 세포 외 산성 pH 에 의하여 voltage-dependent gating 이 뒤바뀌는 특성이 사라지는 것을 보았다. CLC-1 의 3 차원 구조 중 S537 과 그 가까이 있는 아미노산인 Val232 을 exchanger type 의 CLC 구성원 구조에 상응하는 Ile (S537I)과 Glu (V232E)로 치환하면, wild type CLC-1 의 막전압 의존적 common gating 이 사라졌다 (constant-open state). 하지만 S537I/V232E CLC-1 은 Cl^-/H^+ exchanger 의 특성에 해당하는 수소이온 투과성은 보이지 않았다. 이 연구결과들은 CLC-1 의 common gating 작동기전에 대해 새로운 정보를 제공한다. 또한 CLC family 단백질들의 진화과정에서 수소이온의 수송능력 또는 gating 의 pH 감수성에 대한 단서가 될 것으로 기대한다.

본 연구는 *Pflugers Arch.* 2016 Feb;469(2):183-193 에 출판되었음.

주요어 : CLC-1, 선천성 근육긴장증, 염소이온, 수소이온, 전압의존성 이온통로

학 번 : 2014-30672